Alternative Electrochemical Salt Waste Forms, Summary of FY2010 Results

Fuel Cycle Research & Development

SUMMARY

In FY2009, the Pacific Northwest National Laboratory (PNNL) performed scoping studies to down-select two candidate waste forms for spent electrochemical salt, tellurite (TeO_2-based) glasses and high-halide minerals. Both candidates showed promise with acceptable Product Consistency Test (PCT) responses (i.e., an assessment of chemical durability) and immobilization of at least 10 mass% fission product waste stream. These candidates were investigated in FY2010.

Sodalite was successfully synthesized by the sol-gel method. The vast majority of the dried sol-gel consisted of sodalite with small amounts of alumino-silicates and unreacted salt. Upon firing the powders made by sol-gel, the primary phase observed was sodalite with the addition of various amounts of nepheline, carnegieite, lithium silicate, and lanthanide oxides. The amounts of sodalite, nepheline, and carnegieite varied with firing temperature, as did the bulk density of the fired pellets, sol-gel process chemistry, and the amount of glass sintering aid added to the batch. As the firing temperature was increased from 850°C to 950°C, chloride volatility increased, the fraction of sodalite decreased, and the fractions of nepheline and carnegieite increased. This indicates that the sodalite structure is not stable and begins to convert to nepheline and carnegieite under these conditions at 950°C. Density has an inverse relationship with firing temperature. The addition of NBS-1, a borosilicate glass sintering aid, had a positive effect on bulk density and increased the stability of the sodalite structure. A summary data table for FY2010 halide mineral investigations is presented in Table S1.1.

Table S1.1. Summary data for FY2010 halide mineral investigations. "WL" denotes the waste loading (in mass%); "Firing T" denotes the firing temperature (in °C); For the Phase Assemblage, "S" denotes sodalite, "N" denotes nepheline + carnegieite, and "L" denotes lithium silicate phases determined by X-ray diffraction. NL_{Na} and NL_{Cl} denote the sodium and chlorine normalized release, respectively, from the PCT.

Sample ID	Additive / Sintering aid	WL, mass%	Firing T, °C	Density g/cm^3	Phase Assemblage, mass%**	NL_{Cl}, g/m^2	NL_{Na}, g/m^2
S5A	NA	13.7	850	1.57	S 86.4, N 12.4, L 1.2	0.030	3.410
S5B	HNO$_3$	13.7	850	1.34	S 94.7, N 4, L 1.3	0.140	3.780
S6-1%	1% NBS-1	13.6	850	1.73	S 86.5, N 12.1, L 1.4	0.020	3.900
S6-2%	2% NBS-1	13.4	850	1.79	S 85.6, N 12.6, L 1.8	0.020	3.760
S6-5%	5% NBS-1	13.0	850	1.68	S 78.4, N 19.3, L 2.3	0.140	3.520
S6-7%	7% NBS-1	12.7	850	1.92	S 96.5, N 2.5, L 1	0.040	4.450
S5A	NA	13.7	950	1.97	S 54, N 44.1, L 1.9	0.030	3.400
S5B	10% NO$_3$	13.7	950	1.54	S 50.3, N 48.1, L 1.7	0.020	4.540
S6-1%	1% NBS-1	13.6	950	1.91	S 53.9, N 44.8, L 1.4	0.020	4.810
S6-2%	2% NBS-1	13.4	950	2.05	S 58.6, N 39.4, L 2	0.030	4.920
S6-5%	5% NBS-1	13.0	950	2.06	S 51.5, N 46.1, L 2.4	0.030	5.690
S6-7%	7% NBS-1	12.7	950	2.10	S 71.8, N 26.8, L 1.3	0.030	5.320
C1	Ca(NO$_3$)$_2$	15.9	950	1.16	S 53, N 47	0.010	2.890
C2	Ca(NO$_3$)$_3$ + HNO$_3$	15.4	950	1.41	S 69.7, N 30.2	0.030	1.000

At the beginning of FY2010, an in-depth literature review kicked off the tellurite glasses study. The review was aimed at compiling data for chemical durability and mixed chloride incorporation for tellurite glasses. The literature review led the authors to four binary and one ternary systems for further investigation, which include TeO_2 plus the following: PbO, Al_2O_3-B_2O_3, WO_3, P_2O_5, or ZnO. Each system was studied with and without a mixed-chloride simulated electrochemical salt waste stream, and the literature review provided the starting points for the baseline compositions as well as starting points for melting temperature, compatible crucible types, etc. The most promising glasses in each system were scaled up from 5 g scoping study batches to 20 g batches which were analyzed using the PCT. Both as-fabricated samples and samples exposed to PCT were analyzed for phase separation or undissolved

materials. Table S1.2 summarizes the results from FY2010 tellurite glass research efforts. Volatility was rated on a relative scale of 0–4, 0 being negligible and 4 being the most extreme of the glasses melted. Melt pour viscosity was estimated by visual comparison with standards, and density was measured with a helium pycnometer. Phase separation and/or crystallization was measured on a "bulk" scale by visual observations (i.e., glasses where phase separation or crystallization was observed without the need for a microscope) and on a "small" scale by microscopic observations of thin sections. NL_{Na} denotes the sodium normalized release from the PCT.

Table S1.2. Summary data table for FY2010 tellurite glass investigations. T_{melt} is the temperature at which the glasses were melted.

Batch Composition	T_{melt}	Volatility	Viscosity	Density	Phase Separation		NL_{Na}
Mass% additive	°C	0–4	cP	g/cm^3	Bulk	Small	g/m^2
22.0% PbO	705	0	50–100	6.12	-	✔	-
19.8% PbO 10.0% XCl_{20}	705	1	10	5.16	✔	-	0.478
8.8% Al_2O_3 9.0% B_2O_3	720	0	200	4.44	-	✔	-
7.9% Al_2O_3 8.1% B_2O_3 10.0% XCl_{20}*	690	3	50	4.13	✔	✔	6.71
25.0% WO_3	700, 725	0	100	5.92	✔	-	-
22.5% WO_3 10.0 XCl_{20}	675	4	10	5.11	✔	-	10.3
8.9% P_2O_5	675	0	400	5.11	-	-	-
8.1% P_2O_5 10.0% XCl_{20}	675	2	50–100	4.72	✔	✔	86.0
18.0% ZnO	695, 730	0	100	5.49	-	-	-
16.2% ZnO 10.0% XCl_{20}	730	1	10	4.67	-	-	88.9

*The composition of the Echem salts was incorrectly batched in glass P-2

CONTENTS

FIGURES

TABLES

ACRONYMS AND ABBREVIATIONS

ACS   American Chemical Society (chemical meets specifications of the society)

AES   atomic emission spectroscopy

AFCI   Advanced Fuel Cycle Initiative

ASTM   American Society of Testing and Materials, now ASTM International, Inc.

BET   Brunauer Emmett Teller

BSE   backscatter electron imaging

DIW   deionized water

DOE   U.S. Department of Energy

DSC   differential scanning calorimetry

DTA   differential thermal analysis

EA   environmental assessment

Echem   electrochemical separations process

EDS   energy dispersive spectroscopy

FP   fission products

FY   fiscal year

GFR   glass-formation region

IC   ion chromatography

ICP   inductively coupled plasma

ICSD   International Crystal Structure Database

IR   infrared

LOD   loss on drying

LRM   low-activity test reference material

MS   mass spectrometry

NE   (DOE) Office of Nuclear Energy

OES   optical emission spectroscopy

PCT   Product Consistency Test

PDF   Powder Diffraction File

PNNL   Pacific Northwest National Laboratory

PSI   pounds per square inch

RE   rare earth

REO   rare earth oxide

SEI   secondary electron imaging

SEM   scanning electron microscope or scanning electron microscopy

SG   space group

ST	scoping test
T_c	crystallization temperature
T_g	glass transition temperature
T_m	melting temperature
T_x	temperature of the crystallization onset
UDS	undissolved solids
WL	waste-loading
$X\text{Cl}_{10}$	mixed chloride electrochemical waste stream with 10% FP
$X\text{Cl}_{20}$	mixed chloride electrochemical waste stream with 20% FP
XRD	X-ray diffraction

ALTERNATIVE WASTE FORMS

ELECTROCHEMICAL SALT WASTE

1. INTRODUCTION

The Fuel Cycle Research and Development Program, sponsored by the U.S. Department of Energy (DOE) Office of Nuclear Energy (NE), is looking for new alternative waste forms for wastes generated from sustainable nuclear fuel cycles. One such waste results from the electrochemical separations (Echem) in molten KCl-LiCl salt – the spent salt. The Pacific Northwest National Laboratory (PNNL) is investigating candidate waste forms for the Echem spent salt, of which two were selected: high-halide minerals (i.e., sodalite and cancrinite) and tellurite (TeO_2)-based glasses. The results from the fiscal year (FY) 2009 study are presented elsewhere.[1] Both of these candidates showed promise in FY2009, and further testing was performed on these waste forms in FY2010 to investigate the possibility of their use in a sustainable fuel cycle. This report summarizes the results of FY2010 efforts.

The simulated waste composition used in this study is the 20 mass% fission products (FP) waste stream;[2] see Table 1.1. The 20 mass% FP Echem waste stream is designated in this report as XCl_{20}.

Table 1.1. Calculated composition of spent electrochemical salt with 20 mass% FP (XCl_{20}).[2]

Element	Mole Fraction	Mass Fraction
Y	0.0007	0.0020
La	0.0029	0.0127
Ce	0.0045	0.0195
Pr	0.0022	0.0095
Nd	0.0067	0.0301
Pm	0.0003	0.0011
Sm	0.0020	0.0092
Eu	0.0002	0.0011
Gd	0.0002	0.0011
Tb	0.0000	0.0001
Li	0.2219	0.0477
K	0.1603	0.1942
Na	0.0630	0.0449
Rb	0.0006	0.0017
Cs	0.0081	0.0332
Sr	0.0013	0.0036
Ba	0.0030	0.0129
Cl	0.5212	0.5725
Total	1.0000	1.0000
Simplified	Mole Fraction	Mass fraction
Alkali	0.4539	0.3217
Alkaline Earth	0.0044	0.0166
Lanthanide	0.0198	0.0863
Halide	0.5219	0.5754

2. Expanded Background and Literature Review

2.1 Halide Minerals: Expanded Background

This study explored the use of the sol-gel process to produce a ceramic/mineral waste form for the spent electro-refiner salt (XCl_{20}) following the scoping studies conducted in FY2009 to identify and explore

candidate mineral waste forms.[1] Sodalite and cancrinite were identified as the overall best candidate mineral phases for incorporation of XCl_{20}, because of their high concentrations of alkali and Cl, which, when combined, comprise 97 mole% of the waste.[1] The FY2009 scoping studies showed that sodalite can be easily synthesized by the sol-gel process. However, it is produced in the form of a fine powder with particle sizes on the order of a few microns. Due to the small particle size, the powders produced by the sol-gel process require treatment to form a monolith. In this study, the sol-gel powders were pressed into pellets (19–25 mm diameter, 5–10 mm thick) and fired to achieve the desired bulk density (> 90% of theoretical density). Cancrinite, while identified as the best candidate mineral in terms of maximum waste loading, was produced during the sol-gel process but converted to sodalite upon firing. FY2010 efforts focused on two areas: 1) increasing the bulk density of the sodalite waste form, and 2) synthesis of a cancrinite waste form.

To increase bulk density of the sodalite, the firing temperature was varied to determine the maximum firing temperature above which the volatility of Cl became significant. First, the optimum firing temperature was determined based on bulk density, Cl loss, and PCT response. Second, a sintering aid (1–7 mass%) was added in the form of powdered borosilicate glass (NBS-1).[3] The powdered glass was added during the sol-gel process, directly after gel formation before the gel was dried.

Sodalite was the predominant structure that formed during the sol-gel process during the scoping studies of FY2009. Based on the literature, sodalite is more likely to form when the only anion present is Cl-. If significant concentrations of CO_3^{2-}, NO_3^-, or OH- are present then cancrinite can become the preferred structure.[4-6] Chemistry changes were made in an attempt to form cancrinite in place of sodalite. The additions of NO_3^-, CO_3^{2-}, and OH- were examined to determine which if any would form cancrinite instead of sodalite, since cancrinite has a higher theoretical waste loading (23 mass%) than sodalite (13 mass%). The targeted compositions for sodalite synthesis are given in Table 2.1, and those for cancrinite synthesis are given in Table 2.2.

Table 2.1. Target elemental compositions of sodalite formulations (in molar formula units), glass sintering aid and waste loading (mass % addition to original composition). The "Label" is used to identify the samples in later sections. RE denotes the addition of rare earths or lanthanides.

Component	Ideal Sodalite	Sodalite 5A	Sodalite 5B	Sodalite 6 Series
Label	-	S5A	S5B	S6
Al	6.00	6.0	6.0	6.0
Si	6.00	6.0	6.0	6.0
Alkaline earth + RE	-	0.1	0.1	0.1
Alkali	8.00	7.9	7.9	7.9
Cl-, NO_3^-	2.00	2.0	2.0	2.0
O	24.00	24.0	24.0	24.0
NO_3^-/(NO_3^-+Cl-), mass%	-	-	10	-
NBS-1 Glass, mass%	-	-	-	1.0–7.0
Total	46.00	46.0	46.0	46.0
Waste loading, mass%	-	13.7	13.7	12.7–13.5

Table 2.2. Target elemental compositions of cancrinite formulations (in molar formula units), waste loading given in mass %. The "Label" is used to identify the samples in later sections.

Component	Ideal Cancrinite	Cancrinite 1	Cancrinite 2	Cancrinite 3
Label	-	C1	C2	C3
Al	6.00	6.00	6.04	5.94
Si	6.00	6.00	6.00	6.00
Alkaline earth + RE	2.00	0.18	0.16	0.35
Alkali	6.00	8.32	8.26	8.11
Cl^-, NO_3^-, OH^-	4.00	2.53	2.56	2.72
O	24.00	23.79	23.78	23.88
Additive	-	$Ca(NO_3)_2$	$Ca(NO_3)_2 + HNO_3$	$Ca(OH)_2$
Total	48.00	46.82	46.82	47.00
Waste loading, mass%	-	15.86	15.41	14.64

2.2   Tellurite Glasses: Expanded Background

2.2.1   FY2009 Tellurite Glass Efforts

The scoping studies performed in FY2009 with the tellurite glass system revealed the possibility of forming homogeneous glass in the TeO_2-$X$$Cl_{10}$-[$B_2O_3$, Li_2O, and/or Na_2O] glass systems with $X$$Cl_{10}$ loadings up to 19 mass% with a negligible degree of crystallization.[1] (Discussion of the 10 mass% fission products, or FP, simulated waste stream [$X$$Cl_{10}$] used in FY2009 is presented elsewhere.[1]) $X$$Cl_{10}$-loadings of 5–30 mass% were prepared with TeO_2 as the main glass former in a desired ratio, and modifiers (B_2O_3, Li_2O, and Na_2O) were added separately to improve glass processability. The batches were then placed in Pt/5%Au crucibles with Pt/10%Rh lids to reduce the volatility of chlorides during melting and then melted for ~25 minutes at 600–800°C to verify an optimum melting temperature for the tellurite glasses. A melting temperature of 725°C was found to be satisfactory. Two quench methods formed satisfactory glasses: 1) pouring the melt onto a steel plate at room temperature (25°C), and 2) quenching the glass between a steel plate and a platinum sheet with both plates starting at room temperature.

TeO_2-$X$$Cl_{10}$ mixtures were not achieved without significant crystallization (~50 volume % by visual observations), though the crystal fraction in the glass decreased with a higher TeO_2:$X$$Cl_{10}$ ratio. Less off-gas was observed at lower melting temperatures. Crystallinity significantly decreased with the addition of 5 mass% B_2O_3 or Li_2O. A loading of 19.05 mass% $X$$Cl_{10}$ was obtained without crystallization upon quenching in a glass with 4.76 mass% of B_2O_3 with a mass balance of TeO_2.

PCT was performed on these glasses. The PCT leachates were analyzed using ion chromatography (IC), inductively coupled plasma (ICP)-mass spectrometry (MS), and by ICP atomic emission spectroscopy (AES). Although the PCT responses were generally high, these glasses show promise for the target waste stream and require further investigation. Small additions of a co-glass former (i.e., B_2O_3) and glass modifiers (i.e., Li_2O, Na_2O, K_2O) to tellurite resulted in drastically different PCT responses.

The following compositions were proposed in conclusion of the FY2009 literature review and experimentation[1]: "Future work will investigate the solubility of mixed chlorides and performance of tellurite binary and ternary systems including B_2O_3, P_2O_5, Al_2O_3, and/or PbO with or without modifiers, e.g., alkali oxides or transition metal oxides (e.g., ZnO, WO_3, Nb_2O_5)."

2.2.2   Summary of Literature Review

Tellurite glasses were selected over other candidate glass systems such as silicates, lead glasses, and heavy metal oxide glasses ($\geq$ 50 cation% of Pb and/or Bi),[7] for reasons of chloride solubility, low processing temperatures (600–800°C, depending on chemistry), modest glass transition temperature (T_g), and flexible compositional working space. Work in tellurite glasses with various chlorides and with various glass modifiers, intermediates, and co-glass formers is prevalent in the literature. A brief

literature search was performed at the beginning of the FY2009 which led to the study of tellurite glasses. A much more extensive literature survey was continued in FY2010; that data is presented in Appendix A.

2.2.3   Hruby Criterion for Glass Formation Region Estimation

The literature presents various methods for predicting glass formation and stability in terms of the thermal-structural properties. For example, one method is the Hruby Criterion[8] (or K_{gl}) which is defined as:

$$K_{gl} = \frac{T_x - T_g}{T_m - T_c}$$

(1)

where T_x is the crystallization onset temperature, T_g is the glass transition temperature, T_m is the liquidus temperature, and T_c is the maximum of the crystallization exotherm. This method was used to determine tellurite glass forming regions for various binaries and ternaries. Here, the value of $(T_x - T_g)$ has been used as a rough measure of the glass thermal stability when all four parameters of the Hruby Criterion were not available in literature data.[9] In order to achieve compositional flexibility in a particular glass system, it is ideal to start with a large value of $T_x - T_g$. This criterion was implemented in looking for maximum glass stability ranges in the candidate systems when the required parameters were available from the literature.

2.2.4   Expanded Tellurite Glass Literature Study

This section presents a broader and more extensive survey of tellurite glass systems from the perspective of immobilization of the Echem waste. The ideal glass waste form candidate for the current application fulfills the criteria presented below; justification for the rejection or acceptance of each glass system as a candidate for an Echem waste form is discussed within the context of these criteria:

- Waste loading $\geq$ 10 mass% XCl_{20}

- PCT response below Environmental Assessment (EA) glass[10] (a standard reference glass) for which the Li and Na releases are 9.565 $\pm$ 0.735 and 13.346 $\pm$ 0.902 g/L, respectively, and 4.951 $\pm$ 0.537 and 6.841 $\pm$ 0.678 g/m^2, respectively

- Wide range of glass forming ability for tuning properties: can accommodate a wide range of modifiers, intermediates, and co-glass formers

- Less than one volume% phase separation or crystallization in quenched glass

- Melting temperature $<$ 1000°C to minimize volatility of the chlorides during melting

- $T_g \geq$ 300°C or no adverse effects to durability if held above T_g

2.2.5   Key Observations from FY2010 Literature Survey

After reviewing the literature, some key observations were made that helped direct the study are summarized below:

- Tellurite glasses are forgiving as a host for various co-glass formers as well as glass modifiers and intermediates. Tellurite glasses have been demonstrated as hosts for additives from each group of the periodic table, except for noble gases and actinides.

- The literature review revealed many options for candidate types of crucibles when processing tellurite glasses: Al_2O_3, SiO_2, Pt-alloy (e.g., Pt-Rh, Pt-Au), and ZrO_2. Some reviews[11-15] show that dissolution of the crucible into the melt can be advantageous or detrimental to the mechanical and chemical properties of the resultant glass. Stanworth[15] found that zirconia crucibles showed resistance to chemical attack by tellurite glasses.

- Bürger *et al.*[16] demonstrated the need for bubbling the melt with oxygen in order to prevent reduction of the oxides into metals in the case of phosphotellurite glasses. Bubbling was deemed unnecessary with the temperatures and compositions tested in this study.

- Glass modifiers (e.g., alkali, alkaline earths) improve the processability of tellurite glasses (e.g., lower melting point, T_g, viscosity, etc.) at the expense of chemical durability and temperature stability.[13,15]

3.   METHODS

3.1   Sol-Gel Fabrication Method for Halide Minerals

A sol-gel process was used to form sodalite/cancrinite minerals, followed with cold pressing and firing to convert the gel into a monolithic waste form. Figure 3.1 shows a schematic of the sol-gel apparatus. The solution was fabricated as follows:

1) Simulated spent salt (XCl_{20}) was dissolved in deionized water (DIW) – see Figure 3.1-(A).

2) Dissolved salt was heated to ~75°C in the reaction beaker, which was heated by an oil bath. The solution was continuously stirred with a serpentine shaped Pt wire throughout the formation process.

3) Colloidal silica, suspended in a separate solution, was slowly added to the dissolved salt solution – see Figure 3.1-(B).

4) The solution was then gelled by slow addition of sodium aluminate solution – see Figure 3.1-(C).

5) For some of the batches, a sintering aid (1–7 mass%) was added in the form of powdered borosilicate glass (NBS-1) (not shown in Figure 3.1).

6) The gel was stirred and heated for 10–30 min to drive off excess water.

7) Lastly, the gel containing beaker was moved to an oven at 105°C overnight to complete the drying process.

The dried material was a moderately bound fine powder. The amounts of waste simulant, colloidal silica, and sodium aluminate added were determined by the target waste form composition.

Figure 3.1. Schematic of the simplified sol-gel process.

3.2   Preparing Pellets of Halide Minerals

The gels were crushed and pressed into pellets using a combination of press types. First, powders were loaded into a cylindrical die lubricated with an oleic acid. The die was placed in a uniaxial press and pressed to the minimum pressure, 6.89×10^6 Pa (~1,000 pounds per square inch, or PSI), adequate to form and maintain the shape of the pellet (19–25 mm diameter, 5–10 mm thick). Higher pressures created pressure gradients in the pellet, which resulted in cupped pellets after firing. The pellet was then vacuum sealed in a rubber holder and pressed to 4.17×10^8 Pa (60,000 PSI) in an isostatic press.

The pressed pellets were placed on a dense alumina sintering plate and loaded into a furnace. Samples were fired by ramp heating at 1–3°C/min up to the maximum firing temperature of interest (between 600°C and 950°C), held 4–8 hours, and then ramped down to room temperature at 1–3°C/min. A series of samples were calcined at 600°C for 1 hour before firing to evaluate the effect of calcining on bulk density of the waste form.

Ceramic samples were characterized to determine the following: mass loss on firing, green and fired bulk density, crystalline phases (using XRD), microstructure (e.g., pores, grain sizes) and compositional variations (scanning electron microscopy, or SEM, with energy dispersive spectroscopy, or EDS), and PCT response. Mass loss was determined upon calcining and firing using a balance with an accuracy of ± 0.003 g. Mass loss was monitored to help evaluate volatility of Cl.

3.3   Tellurite Glass Fabrication

High purity source chemicals (listed in Appendix B) were carefully weighed targeting a glass mass of 5.0000 or 20.0000 g (after loss on drying) for scoping and scale-up batches, respectively, on an analytical balance (±0.1 mg precision) and placed into an agate mortar and milled with an agate pestle. This method proved to be efficient at mixing the powders and allowing for collection following the mixing. Unlike the FY2009 experiments, the Echem simulant was not prepared in a batch and added to glass forming compounds, but all salts were kept separate and added to the batch according to each individual batch recipe. Tellurite and chloride powders (for waste-loaded glasses) were weighed before the secondary glass-forming components were weighed. The mixtures were transferred to crucibles with Pt/10%Rh lids and placed in a furnace within a fume hood for melting. The crucible materials were Pt/5%Au for 5 g batches and Pt/10%Rh for 20 g batches. Depending on the batch composition, the melting temperature varied between 680°C and 730°C (several unsuccessful batch experiments were processed at 980°C). Most glasses were successfully melted after one 30-minute heat treatment at the desired temperature. For glasses that required additional heat treatments, multiple melting temperatures are listed in Table 4.5 in Section 4.3. Melts were quenched by pouring onto an Inconel® plate within the fume hood. Visual volatilization observations were recorded after removing the lid from the crucible inside the furnace.

Batches were processed in two types of batch experiments: scoping tests (STs) and product consistency tests (PCTs).   Scoping tests investigated glass formability of the compositions chosen based on the literature review in 5 g batches; the samples are labeled S-#, where # is the number in the list of batches processed chronologically. Glass compositions and processing conditions were modified based on results and further literature review. Selected glasses were scaled up to 20 g batches for PCTs, labeled P-#, where # is the number in the list of batches processed chronologically. The final glasses prepared for PCT are listed in Table 4.5 with compositions (mass%), melting temperatures and additional observations.

Two Deltech® top-hat furnaces were used for melting glass. It was discovered that the first furnace typically obtained 25–30°C higher than the programmed set point within the range of melting temperatures. The second furnace obtained temperatures roughly 10°C cooler than the programmed set point. This affected the processing of glasses P-2 and P-4, which will be discussed in Section 4.3. Glasses without waste simulant additions were first fabricated and tested. Processing conditions that produced satisfactory glasses from compositions without waste simulant addition were used to fabricate glasses with waste additions and, if necessary, were modified in subsequent batching if an initial batch was unsuccessful. When adding the simulant at a particular loading, the ratios between the mass fractions

of TeO_2 and the secondary glass components established in the host compositions were maintained. That is, the waste displaced the starting glass in equal ratio.

Initial pour viscosity was estimated visually by comparison to viscosity standards (Cannon Instrument Company and Brookfield) which covered the range 5.635×10^{-4}–5.62×10^{-1} Pa·s (0.5635–562 cP).

Due to the hygroscopic nature of P_2O_5, the source chemical bottle was stored in a nitrogen-purged glove box, and small aliquots of that source chemical were removed in glass scintillation vials and stored in a polycarbonate vacuum desiccator to extend the shelf life of the powder outside of an inert atmosphere.

3.4 Waste Form Characterization

3.4.1 Optical Microscopy

Glasses were characterized using three optical (light) microscopes: a Leitz Orthoplan, an Olympus SZH10, and an Olympus PMG-3. In some cases, a polished cross-section of the glasses was observed in reflected or transmitted light, depending on the opacity of the sample, but most of the time, the glasses were observed as-quenched. Also, low-magnification optical micrographs were collected of the bulk glasses, of the crucible, and of the pour plate surface after most melts for process comparisons between compositions.

3.4.2 Density Measurements: Helium Pycnometry

The density of each tellurite glass for PCT measurements was measured with a Micrometrics AccuPyc 1330 helium gas pycnometer. The pycnometer was configured to perform five purges and five measurements during calibration and sample analysis. The pycnometer was calibrated using a standard of known volume (0.7185268 cm^3) and the equilibrium rate was 0.0050 psig/min. Mass values were measured with an analytical balance (± 0.0003 precision). If phase separation or inhomogeneity was observed in the specimen, multiple samples from the specimen were analyzed and the values averaged.

3.4.3 Density Measurements: Bulk Density

Bulk density was measured by taking accurate mass and geometric volume measurements (average height and diameter) of the ceramic pellets before firing (green density) and after firing (sintered density). Mass readings were recorded using an analytical balance with a precision of ± 0.003 g, and volumetric measurements were taken with digital calipers with a precision of ± 0.01 mm. Efforts were made to minimize cupping of the pellets; however, some cupping was observed, leading to some error in fired densities measured with this method. Archimedes' method was used to measure density in these cases since it less sensitive to irregularly shaped samples.

3.4.4 Density Measurements: Archimedes Method

Archimedes' method was also performed to measure density, bulk density excluding open porosity of the fired pellets; this method accommodates irregularly shaped objects, so pellet cupping does not introduce error into the measurements. Samples were weighed dry, then submerged in and saturated with ethanol. By taking all three mass measurements, open porosity and bulk density were determined. The temperature of the ethanol was monitored and used to calculate its density. Before the submerged and saturated weights were taken, the samples were allowed to sit in ethanol under lab vacuum conditions for 20 minutes to remove all air from open pores of the pellet. The balance used for the measurements has a precision of ± 0.0003 g.

3.4.5 X-Ray Diffraction

The X-ray diffractometer (XRD) used for structure and phase analysis was a Bruker D8 Advanced equipped with a Cu Kα target set to a power level of 40 kV and 40 mA. The detector used was a position-sensitive detector with an angler range of 3° 2θ. Typical scan parameters used for sample analysis were 5–110° 2θ (sometimes 5–70° 2θ) with a step of 0.015° 2θ and a 0.3 second dwell at each step. JADE™ 6, EVA, and Bruker AXS© Topas 4.2 software were used to identify and quantify phase assemblages.

For the halide minerals, pellets were ground into a fine powder and placed into the XRD to measure the crystal structure of the phases present in the waste form. Tellurite glass samples were ground to a fine powder by one of two methods: 1) crushing in a tungsten carbide milling chamber of an Angstrom Laboratory Ring Pulverizer and 2) crushing in a Diamonite mortar and pestle depending on the chemicals present in the glass, i.e., if hazardous chemicals were present in the specimen (e.g., Pb), the mortar and pestle was used to minimize the spread of these chemicals.

3.4.6   Scanning Electron Microscopy & Energy Dispersive Spectroscopy

A JEOL JSM-5900 SEM was used to capture micrographs of the halide minerals and tellurite glass powders using secondary electron and backscatter electron imaging (SEI and BSE, respectively). EDS was performed using an EDAX Li-drifted Si detector.

Halide mineral pellets were either fractured or cross-sectioned, polished, and then placed into the SEM to examine morphology, grain size, and perform elemental analysis of the phases. Micrographs were captured at various magnifications. EDS was performed without standards and is considered semi-quantitative.

Tellurite glass powders (of the same size fraction used for PCT, -100/+200 mesh or -149/+74 µm) before and after PCT were analyzed to get a visual comparison of the glasses as well as compositional analysis. A Robinson backscatter detector was used to look for atomic-number contrast in the specimens. The working distance used for the analysis was 12 mm, and a spot size of 37–40 (unit less) was used to obtain good count rates (~2000–2500 counts per second) for EDS analysis of the glasses before and after PCT (collection time of 100 seconds for each specimen). Quartz (as verified by XRD) was used as an oxygen standard to calibrate for EDS.

3.4.7   Product Consistency Test

The PCT was performed on the halide minerals and 20-g tellurite PCT batches according to Test Method B (PCT-B) of ASTM Standard C 1285-02.[17] In FY2009, unsensitized type 304L stainless steel PCT vessels were used in the PCT. It was discovered during the cleaning of these vessels that they had undergone moderate to heavy corrosion during the PCTs; this was attributed to the low pH of the leachate solutions (caused by chlorine release from the glasses). PCT-B has procedural flexibility that allows the use of perfluoroalkoxy-tetrafluoroethylene-fluorocarbon vessels, which are not susceptible to corrosion; it was therefore concluded that PCT-B was most appropriate to test chemical durability for the glasses in this study. The PCT test performed in FY2010 on these materials included single samples of 12 different halide mineral samples, triplicates for each of the ten 20 g PCT tellurite glasses, three replicates of the low-activity test reference material (LRM) standard glass,[17] and two deionized water DIW blanks.

Portions of 9–10 g were set aside from the 20-g samples of the PCT tellurite glasses. These tellurite glass portions along with the minerals were crushed manually in a tungsten carbide milling chamber and sieved to US Standard ASTM -100/+200 mesh (149–74 µm) in stainless steel sieves. Specimens were cleaned, according to the procedure set out in PCT-B, in glass scintillation vials. Filtered rinsate samples were retained from the cleaning step with ASTM Type 1 water (DIW) and analyzed for chloride (Cl⁻) content by ion chromatography (IC).

The Teflon vessels were scrubbed thoroughly in soap and water and rinsed with DIW. Next, they were boiled in ASTM Type 1 water for at least one hour and dried overnight at $90 \pm 10°C$. The chosen leachant was ASTM Type 1 water, and the test duration was 7 days $\pm$ 3.4 hours in a $90 \pm 2°C$ oven.

The PCT leachates were removed from their vessels and filtered through a 0.45-µm filter to remove particulates. A small aliquot was removed for pH measurements. The remaining leachates were put into plastic vials and acidified with 1% concentrated HNO_3 (by volume). They were then analyzed, using: IC for dissolved chloride; ICP optical emission spectroscopy (OES) for Al, B, Pb, Zn, P, Ba, Ca, Si, Na, and Li; and ICP-MS for Cs, Ce, W, Te, Pr, Nd, Sm, and La. The results are summarized in Section 4.3.4.

Microsoft Excel 2007 was used for the processing of ICP-OES analysis data. The normalized concentration, NC_i, was calculated for comparison with the EA glass,[10] and is expressed as:

$$NC_i = c_i(\text{sample}) / f_i \tag{2}$$

where $c_i(\text{sample})$ is the concentration of element "i" in the solution (g_i/L, determined by ICP-AES, ICP-MS, or IC), f_i is the mass fraction of element "i" in the unleached waste form as batched (unit less) and the result, NC_i, is $g_{\text{waste form}}$/L_{leachant}.

The normalized release, NL_{Li}, was calculated according to the expression:

$$NL_i = NC_i/(SA/V) \tag{3}$$

where SA/V is the estimated surface area of the final waste form divided by the leachate volume (m^2/L). This ratio was calculated separately for each replicate due to the variability in the glass density between different samples. This calculation was performed assuming identically-sized spherical glass particles and a Gaussian particle size distribution. The average diameter of -100/+200 mesh particles (111.5 µm) was used, as it introduces no significant error.[17] The halide minerals were also measured by Brunauer Emmett Teller (BET) technique to determine the exact surface areas of the particles that had been sieved (-100/+200 mesh).

The measured densities of the tellurite glasses were considerably higher ($\geq$4.13 g/cm^3) than a traditional borosilicate glass (~2.65 g/cm^3), and thus the units used for PCT were renormalized to g/m^2 versus the normal g/L units.

4.   RESULTS & DISCUSSION

4.1   PCT Validation

Several criteria are set forth to validate PCTs. The test period should be controlled to within 7 days ± 3.4 hours, and the mass lost during the PCT should be less than 5% of the total mass (sealed PCT vessel with leachant and glass).[17] In addition to these criteria, Ebert and Wolf[18] presented ranges of leachate pH and element concentrations to apply to PCTs performed on the LRM as a measure for evaluating the accuracy of PCTs performed with the LRM glass as a reference. The expected leachant pH should be 10.92 ± 0.43, and the concentrations (mg/L) of B, Na and Si should be 26.7 ± 7.2, 160 ± 13, and 82.0 ± 12.7, respectively. All PCTs were controlled within the 7 days ± 3.4 hour period, and the total mass loss did not exceed 5% for any PCT. The leachate pH for the FY2010 PCTs performed on LRM was 10.82 ± 0.02, and the raw ICP results (mg/L) for B, Na, and Si were 26.8 ± 0.4, 162 ± 4, and 81.0 ± 0.4, respectively. Therefore, the FY2010 PCT data reported here have been deemed valid.

4.2   Halide Minerals

4.2.1   Halide Minerals: Sol-Gel Process

The gel formation process was the most effective for the S5A and S6 series and took place over a period of a few minutes. All the other sodalite and cancrinite batches involved additives that were combinations of the anions NO_3^-, OH^- or CO_3^{2-}. When adding NO_3^- to the batch, the gel process was delayed somewhat followed by rapid formation of a gel that had noticeably high viscosity compared to batches with no additives. The addition of HNO_3 resulted in a much more acidic solution in the beginning of the sol-gel process. Since adding the basic $NaAlO_2$ solution was the last step of the process, it appeared that a portion of the solution was needed to neutralize the acid and initiate gelation, upon which gel rapidly crashed out of the solution. Adding in OH^- and CO_3^{2-} had similar effects on the gel formation process, but there was no delay in the gelation upon addition of $NaAlO_2$. These results indicated that a single anion, Cl^-, enables the most gradual and controlled gel formation process. Changes in pH also affect the gel-formation process. The addition of OH^- and CO_3^{2-} did produce some cancrinite during the gel formation process; however, sodalite was always the dominate phase formed by the sol-gel process with the chemistries that were investigated.

4.2.2   Halide Minerals: Pellet Pressing and Firing Process

Cupping was observed on fired pellets with increased pressure during uniaxial pressing. This indicates that significant pressure gradients were produced by the uniaxial pressing process. Because of this, uniaxial pressures were minimized to reduce cupping of pellets. Also, pellets pressed in the uniaxial press alone expanded during the firing process or cracked. So uniaxial pressing was followed by isostatic pressing to 3.45×10^8–4.17×10^8 Pa (50,000–60,000 PSI). Fired pellets that had undergone isostatic pressing shrank during firing, indicating that sintering and densification had occurred.

The Sodalite 6 series pellets were yellowish in color, unlike all other pellets, which were white with a few small specks of bluish colored crystals. The yellowish color was assumed to be introduced by the glass sintering aid. The Sodalite 6 series was also noticeably harder in terms of fracture toughness when attempting to fracture the pellets for further testing. *Note: fracture toughness was not measured in any way; this is a qualitative observation only.*

4.2.3   Halide Minerals: Scanning Electron Microscopy

SEM images were collected on fracture surfaces and on polished cross sections to examine the sintering behavior and presence of minor phases not detected by XRD. The fracture surfaces of the sodalite pellets show grains have fused to one another; however, the pore space is still significant (see example in Figure 4.1-A). The grain size is on the order of a few microns, which is similar to the size before firing. Halite, or alkali chlorides, minerals were observed as large, faceted crystals as shown in Figure 4.1-B. The polished cross-sections show areas of open porosity between grains (see dark spots in Figure 4.1-C). In addition, larger voids are seen throughout the samples, (e.g., in the specimens with glass additions – see Figure 4.1-D). The Sodalite 6 series shows less grain-boundary porosity, although there are still larger voids throughout the samples.

A rare-earth (RE)-rich phase was observed as a trace phase at high magnifications, as shown in Figure 4.1-C. The RE-rich crystalline phase was too small to quantify elementally by EDS measurements. The phase is assumed to be either a rare earth oxide or rare earth silicate.
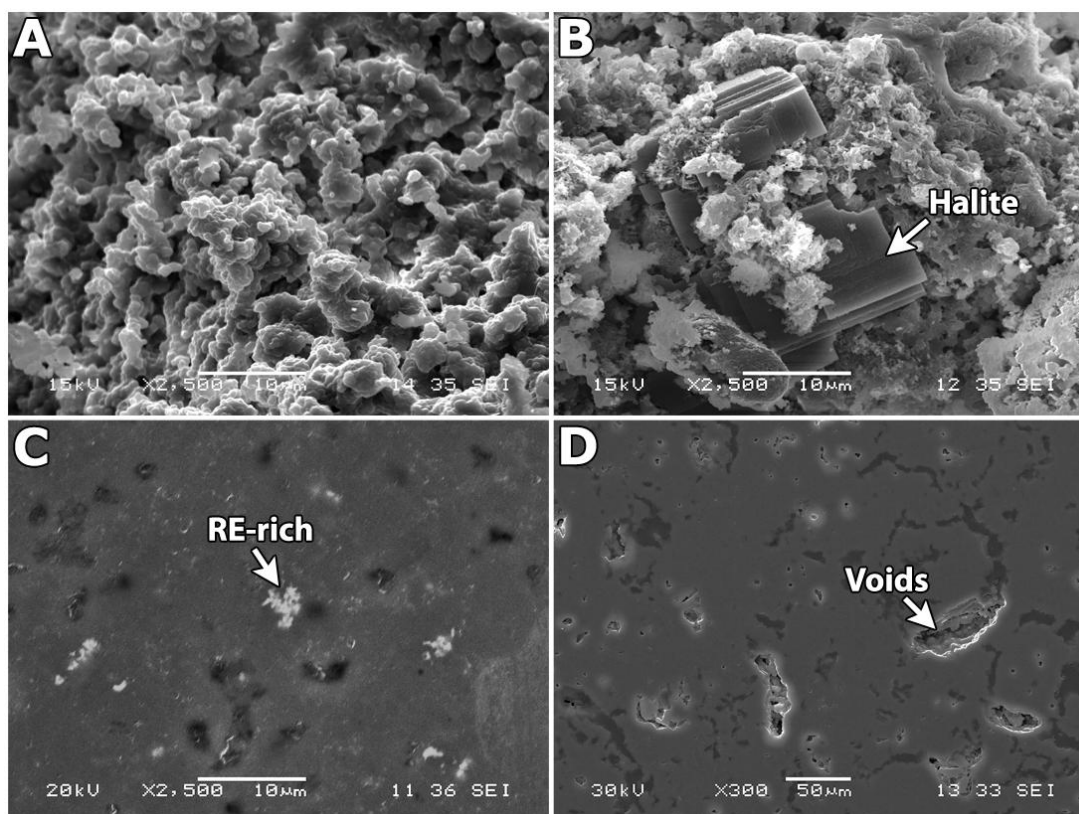
Figure 4.1. SEI micrographs of different halide mineral specimens. (A) Typical fracture surface of pellets captured at 2500× (S4 fired at 850°C for 4 hours).[1] (B) Typical appearance of halite present in the pellets captured at 2500× (S3 850°C for 4 hours).[1] (C) Typical polished cross section captured at 2500× (S5A fired at 950°C for 4 hours). (D) S6 with 1 mass% NBS-1 glass cross-section captured at 300× showing void spaces present in the sintered pellet (fired at 950°C for 4 hours).

4.2.4   Halide Minerals: Pellet Densities

Table 4.1 shows the bulk densities, measured geometrically and by Archimedes' method. An increase in firing temperature, from 850°C to 950°C, significantly increased the density of the samples. The most dramatic increases were seen for samples that didn't have NBS-1 as a sintering aid. The addition of NBS-1 had about the same effect on density as firing temperature. S5A has a measured density of 1.97 g/cm^3 at a firing temperature of 950°C, which is near 90% of theoretical density of sodalite (2.27 g/cm^3). Similar density was observed for S6 with 7 mass% NBS-1, at 1.92 g/cm^3 at a firing temperature of 850°C. At a firing temperature of 950°C, S6 with 7 mass% NBS-1 had a density of 2.10 g/cm^3, which is 92% of theoretical density.

Measured densities of C1 and C2 were very low at 1.16 and 1.41 g/cm^3, respectively. S5B was also quite low at 1.54 g/cm^3. NO_3^-, OH^-, and/or CO_3^{2-} were added to the solutions of S5B as well as C1 and C2. The low measured densities could be related to the instability of these anions versus Cl^-.

Geometric densities were measured initially, but due to discrepancies arising from pellet cupping, the geometric measurements were abandoned and Archimedes' method was used for all measurements. Cupping resulted in an artificially low density measured by the geometric method because the measured height of the pellet was larger than the actual height, a phenomenon supported by the slightly higher densities measured by Archimedes' method when taking open porosity into consideration during the measurement.

Table 4.1. Measured densities according to firing temperature, in g/cm^3. Percentages listed in the table show the effect of adding of NBS-1 glass sintering aid (in mass%) to the base composition.

Sample ID	Temperature	Bulk density (±0.01)	
	°C	Geometric	Archimedes
S5A	850	1.50	1.57
S5B	850	1.27	1.34
S6 + 1%	850	1.63	1.73
S6 + 2%	850	1.71	1.79
S6 + 5%	850	1.52	1.68
S6 + 7%	850	1.84	1.92
S5A	950	NA	1.97
S5B	950	NA	1.54
S6 + 1%	950	NA	1.91
S6 + 2%	950	NA	2.05
S6 + 5%	950	NA	2.06
S6 + 7%	950	NA	2.10
C1	950	NA	1.16
C2	950	NA	1.41

4.2.5   Halide Minerals: X-Ray Diffraction

XRD was performed on fired pellets before and after the PCT for samples fired to 850°C and 950°C: results are shown in Table 4.2, and the phase details are shown in Table 4.3. Sodalite was the dominate phase in all of the samples, followed by nepheline, carnegieite low, and Li_2SiO_3. The results show that increased firing temperatures led to volatility of Cl, instability of the sodalite structure, and the increased formation of sodium-alumino-silicates ($NaAlSiO_4$), namely nepheline and, to lesser extent, carnegieite low, shown in Table 4.2 as ΔSodalite. Increasing the firing temperature from 850°C to 950°C resulted in sodalite loss between 25–44 mass% depending upon the batch. Increased $NaAlSiO_4$ accounts for 97–100 mass% of the sodalite mass lost due to increased firing temperature. The addition of NO_3^- to the S5B batch resulted in more instability of the sodalite structure. NO_3^- appears more volatile than Cl^- in the sodalite structure. On the other hand, the addition of NBS-1 in the S6 series resulted in an increased retention of sodalite at high temperatures (≤ 6 mass% more).

Table 4.2. Phase assemblage of different halide mineral samples measured by XRD (in mass%). "S" labels denote sodalite samples and "C" labels denote cancrinite samples.

Sample ID	Firing temperature, °C	Carnegieite low	Li_2SiO_3	Nepheline	Sodalite	ΔSodalite 850°C–950°C
S5A	850	3.5	1.2	8.9	86.4	
S5A	950	4.6	1.9	39.5	54.0	32.4
S5B	850	3.7	1.3	0.3	94.7	
S5B	950	6.6	1.7	41.5	50.3	44.4
S6-1%	850	1.4	1.4	10.7	86.5	
S6-1%	950	1.1	1.4	43.7	53.9	32.7
S6-2%	850	1.0	1.8	11.6	85.6	
S6-2%	950	0.7	2.0	38.7	58.6	27.0
S6-5%	850	0.7	2.3	18.6	78.4	
S6-5%	950	0.6	2.4	45.5	51.5	26.9
S6-7%	850	1.5	1.0	1.0	96.5	
S6-7%	950	1.8	1.3	25.0	71.8	24.7
C1	850	5.0		14.6	80.4	
C1	950	10.0		37.0	53.0	27.4
C2	850	4.9		17.2	77.9	
C2	950	13.2		17.0	69.7	8.1

Cancrinite samples all converted to sodalite upon firing to temperatures of 750–950°C. The amount of cancrinite before firing varied from 16–22 mass%. Upon firing, the cancrinite became unstable and converted to sodalite, nepheline, and carnegieite low. Li_2SiO_3 was not observed by XRD for the cancrinite formulations. The concentration of sodalite was lower compared to the sodalite formulations, probably because of the additions of anions.

The concentration of sodalite plotted as a function of the fraction of NBS-1 glass sintering aid added to the batch is shown in Figure 4.2. Figure 4.2 reveals two phenomena: (1) the sodalite concentration increased with the addition of NBS-1 at 850°C and 950°C and (2) NBS-1 glass appeared to have a stronger effect as a function of increased firing temperature. The S6-5% samples appear to be outliers at both 850°C and 950°C and were omitted from the fitted trend lines which are shown as a guide to the eye (the data are not sufficient to model). More data and retesting of S6-5% are needed to confirm the effect of the NBS-1 glass. However, this data does show a potential area to improve the sodalite waste form.
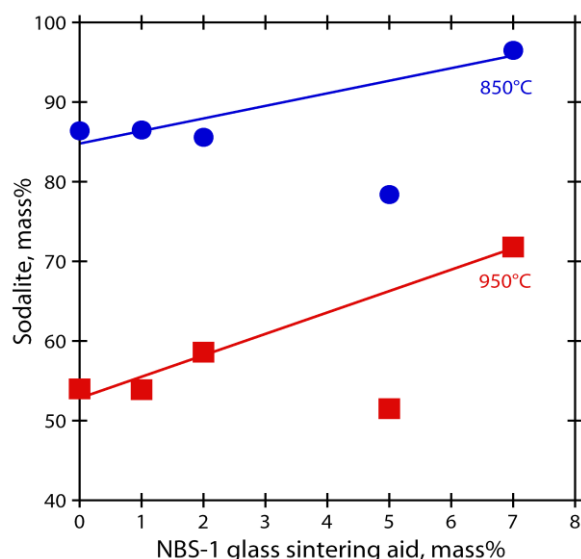
Figure 4.2. Sodalite concentration as function of temperature and NBS 1 glass additive.

Table 4.3. Summary of phases identified in the halide minerals. The table shows powder diffraction file (PDF) and/or International Crystal Structure Database (ICSD) identifications, the space group (SG), lattice ("Trig.", "Orth.", "Hex.", and "Cub." denote trigonal, orthorhombic, hexagonal, and cubic lattices, respectively), unit cell dimensions (a, b, c), and references for the patterns.

Phase ID	PDF#, ICSD#	SG	Lattice	Dimensions (a, b, c)	Reference
Cancrinite	83-1183, 80298	P3 (143)	Trig.	12.624, 12.624, 5.170	Lindner et al.[19]
Carnegieite low	44-1496, 73511	Pb21a (29)	Orth.	10.261, 14.030, 5.157	Withers & Thompson[20]
Li_2SiO_3	83-1517, 100402	Cmc21 (36)	Orth.	9.396, 5.396, 4.661	Seemann,[21] Hesse[22]
Nepheline	76-2465, 37354	P63 (173)	Hex.	10.06, 10.06, 8.42	Foreman & Peacor[23]
Sodalite	37-0476, 41188	P-43n (218)	Cub.	8.879, 8.879, 8.879	Beagley et al.[24]

4.2.6   Halide Minerals: Product Consistency Test

Normalized releases are given in Table 4.1 in terms of g/m^2 for PCT-B tests conducted for 7 days. The normalized releases are high and are attributed to high measured surface areas measured by BET; the normalized releases based on geometrically calculated surface areas are an order of magnitude above the

LRM standard reference material. The surface area of the PCT powders measured by BET is, on average, an order of magnitude larger, at 0.64 m^2/g, than the geometric surface area calculated by assuming a particle size of between -100/+200 mesh, 1.99×10^{-2} m^2/g. If the normalized release is calculated based on BET surface area of the samples, then the normalized releases are similar to the normalized release rates for the LRM glass. However, in order to compare the samples to a standard waste form with zero open porosity (i.e., glass), geometric surface area is more appropriate. More complete sintering would improve performance of the waste form by removing the high accessible surface area.

The PCT powders were analyzed post-PCT by XRD, and no corrosion products were observed. The XRD did reveal a systematic change in which carnegieite and nepheline concentrations went down slightly and sodalite went up relatively after PCT. This indicates that the NaAlSiO$_4$ phases leach preferentially in relationship to the sodalite phase. The concentration of Cl$^-$ is also very low in relationship to the release of alkali.

The rinsate was collected during the washing step of the sieved powders and was analyzed by IC for Cl$^-$ to determine whether a soluble chloride, i.e., halite, was present in the waste form. The results showed that most of the samples released ~0.1 to 0.2 mass% of the total Cl$^-$ during the wash step of the PCT procedure (i.e., rinsing). Three samples, S5B-850°C, S6-5%-850°C, and S6-7%-850°C, have significantly higher releases of Cl$^-$ during the washing step, at 1.5, 1.4, and 1.4 mass% total Cl$^-$, respectively. It is assumed that this release of soluble Cl$^-$ is due to unreacted halite present in the samples along grain boundaries. The release rates are low enough that the salt phase they represent in the samples is below the detection limit of the XRD analysis performed on the pellets.

Table 4.4. NL_i rates for PCT-B test for 7 days, where i = Al, Cl, Li, K, Si, and Na (in g/m^2). Percentages shown are the mass% additions of NBS-1 to the original specimen (that did not contain NBS-1).

Sample ID:	S5A	S5B	S6-1%	S6-2%	S6-5%	S6-7%	LRM	
Fired, °C:	850	850	850	850	850	850	NA	
Al	0.47	0.35	0.20	0.11	0.08	0.32	0.12	
Cl	0.03	0.14	0.02	0.02	0.14	0.04		
Li	1.96	1.88	2.41	2.11	2.19	3.13		
K	0.60	1.54	0.49	0.60	1.25	0.98		
Si	0.35	0.38	0.64	0.97	0.90	0.61	0.14	
Na	3.41	3.78	3.90	3.76	3.52	4.45	0.51	

			Table 4.4 (continued)					
Sample ID:	S5A	S5B	S6-1%	S6-2%	S6-5%	S6-7%	C1	C2
Fired, °C:	950	950	950	950	950	950	950	950
Al	0.30	0.10	0.20	0.08	0.07	0.27	1.12	0.37
Cl	0.03	0.02	0.02	0.03	0.03	0.03	0.01	0.03
Li	1.78	2.44	2.55	4.89	4.10	2.76	1.45	0.28
K	0.15	0.55	0.35	0.51	0.68	0.54	0.11	0.60
Si	0.64	1.16	0.92	1.62	1.84	0.87	0.14	0.14
Na	3.40	4.54	4.81	4.92	5.69	5.32	2.89	1.00

4.3   Tellurite Glasses

4.3.1   Tellurite Glasses: Fabrication Summary

Pertinent batching data and observations are given in Table 4.5 for all glasses made and tested with the PCT in this study. Melting temperatures varied between 675°C and 730°C depending on glass composition. In the case of waste-loaded glasses, volatilization was visible after the melting process and removal of the crucible lid. Off-gases were not observed leaving any of the host glasses (0% XCl$_{20}$) after lid removal, but a condensate phase was present in the case of the PbO and WO$_3$ glasses. For most waste loaded glasses, a residue formed on the quench plate that varied between a slight discoloration on the

plate to a white film. Small black spots were also present after quenching PbO host and waste-loaded compositions, WO_3 waste-loaded glasses, and P_2O_5 host glasses.

As stated in Section 3.3, the use of the second furnace affected the processing of glasses P-2 and P-4. The observation of the second furnace's cooler operating temperature relative to the first furnace was not made until the melting of glass P-4. As a result, T_{melt} for glass P-2 was 30°C less than was intended for processing, and P-4 was subjected to two heat treatments.

Volatility was rated on a relative scale of 0–4, 0 being not observed and 4 being thick white fume coming from the crucible upon removing the lid. The estimated pour viscosity (in centipoise) and the average density (g/cm^3) are included. The densities were measured using a helium pycnometer (see Section 3.4.4) to 5 significant digits and values averaged; the overall standard deviation was ±0.033 g/cm^3. The glasses with the highest variation in measured density due to phase separation and/or crystallization were P-12 (±0.033), P-13 (±0.011), P-14 (±0.009), and P-5 (±0.007) (values listed in g/cm^3). Phase separation and/or crystallization was measured on a "bulk" scale by visual observations (i.e., glasses where phase separation or crystallization was observed without the need for a microscope) and on a "small" scale by microscopic observations of thin sections. The calculated sodium release (NL_{Na}) (see Section 4.3.4 for elaboration) is also listed here for comparison.

Table 4.5. Summary results for tellurite glasses analyzed by the PCT. The "Glass" column lists those glasses batched on a 20-g scale for the PCT. Batch composition of each glass is listed in mass% additive; the balance is TeO_2. With the exception of P-2, the composition of XCl_{20} is found in Table 1.1. The melting temperature is denoted T_{melt}. The overall deviation associated with the density measurements is ±0.015 g/cm^3.

Glass	Batch Composition mass% additive	T_{melt} °C	Volatility 0–4	Viscosity cP	Density g/cm^3	Phase Separation Bulk	Small	NL_{Na} g/m^2
P-8	22.0% PbO	705	0	50–100	6.12	-	✔	-
P-11	19.8% PbO 10.0% XCl_{20}	705	1	10	5.16	✔	-	0.478
P-7	8.8% Al_2O_3 9.0% B_2O_3	720	0	200	4.44	-	✔	-
P-2	7.9% Al_2O_3 8.1% B_2O_3 10.0% XCl_{20}*	690	3	50	4.13	✔	✔	6.71
P-9	25.0% WO_3	700, 725	0	100	5.92	✔	-	-
P-12	22.5% WO_3 10.0 XCl_{20}	675	4	10	5.11	✔	-	10.3
P-5	8.9% P_2O_5	675	0	400	5.11	-	-	-
P-14	8.1% P_2O_5 10.0% XCl_{20}	675	2	50–100	4.72	✔	✔	86.0
P-4	18.0% ZnO	695, 730	0	100	5.49	-	-	-
P-13	16.2% ZnO 10.0% XCl_{20}	730	1	10	4.67	-	-	88.9

*The composition of the Echem salts was incorrectly batched in glass P-2 (see Appendix E)

4.3.2   Tellurite Glasses: Scanning Electron Microscopy

Since it was difficult to capture the difference in appearance of the tellurite glasses before and after PCT because most of the glasses were colorless, they were analyzed by SEM at the same magnification – see Figure 4.3. All ten glasses appear very similar before PCT, and some appear very different after PCT, primarily the ZnO and P_2O_5 glasses which devitrified and formed porous discs due to high dissolution during the PCT and had to be broken and ground up for SEM imaging. Pre-PCT glass samples were consistent with each other in shape and size.
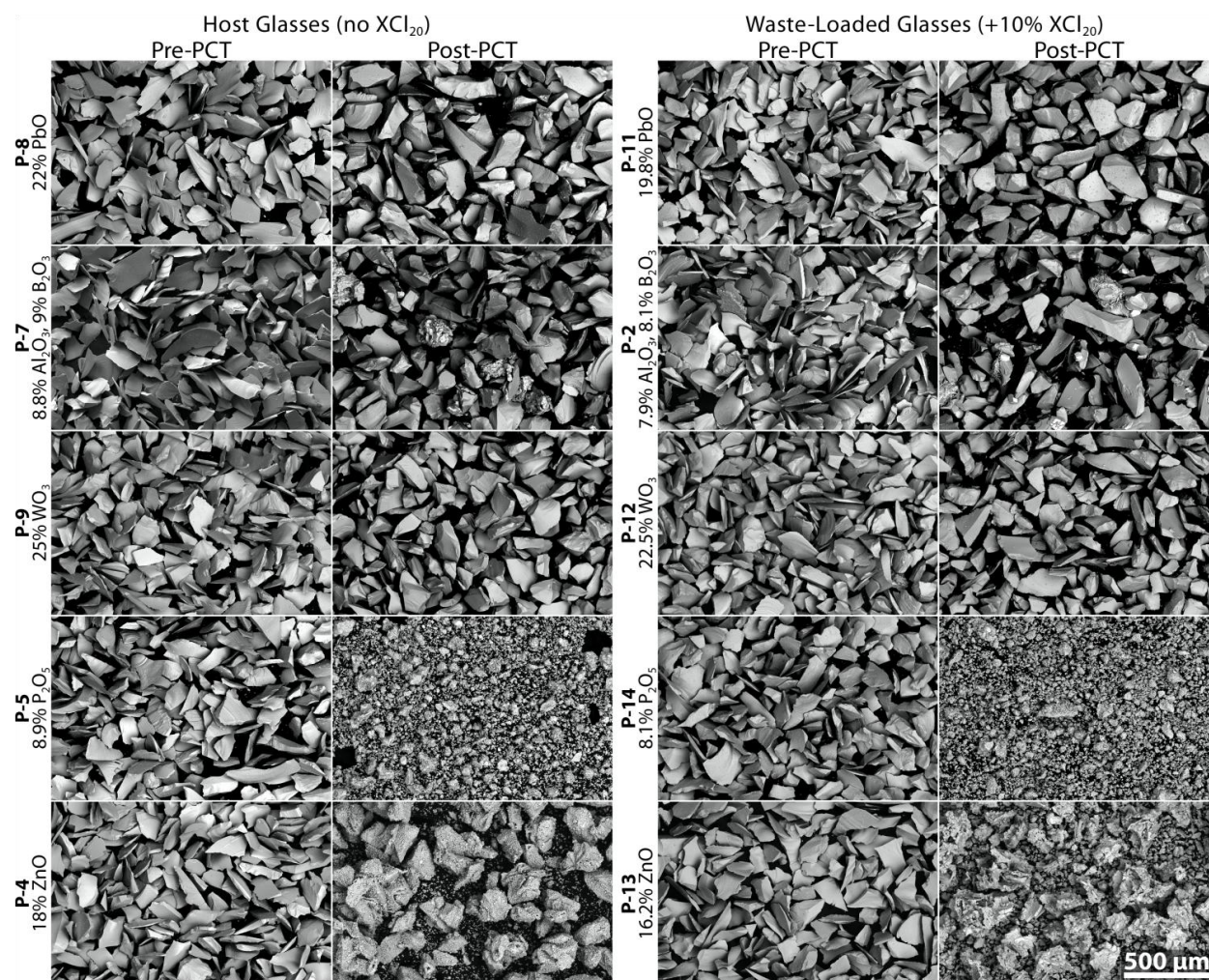
Figure 4.3. SEM micrographs of ten tellurite glasses before and after analysis by PCT. All micrographs were captured at the same magnification, so the scale-bar in the bottom right corner is valid for all micrographs.

EDS analysis was used to measure the composition of the glasses before and after PCT, and the values were then compared with the target values – see Figure 4.4. Different shell energies were used to collect EDS information for the different elements: K-shell energies were used for O, Al, Na, Cl, K, and P; L-shell energies were used for Te, Cs, Ba, La, Ce, Pr, Nd, Sm, and Zn; and M-shell energies were used for Pb and W. In Figure 4.4, the values for the primary additives were normalized out from the as-collected EDS data and presented next to the targeted data. The largest anomalies in the data are the large differences between the targeted/measured WO_3 levels in the WO_3 glasses and the host and waste-loaded (WL) post-PCT measured data for the P_2O_5 glasses. WO_3 is known to cause increase volatility in glass, which was observed when melting the chloride-loaded WO_3 glass (P-12) (see Table 4.5), but the measured WO_3 values are higher than the targeted suggesting the opposite effect, unless the addition of WO_3 to TeO_2 causes preferential TeO_2 volatility.
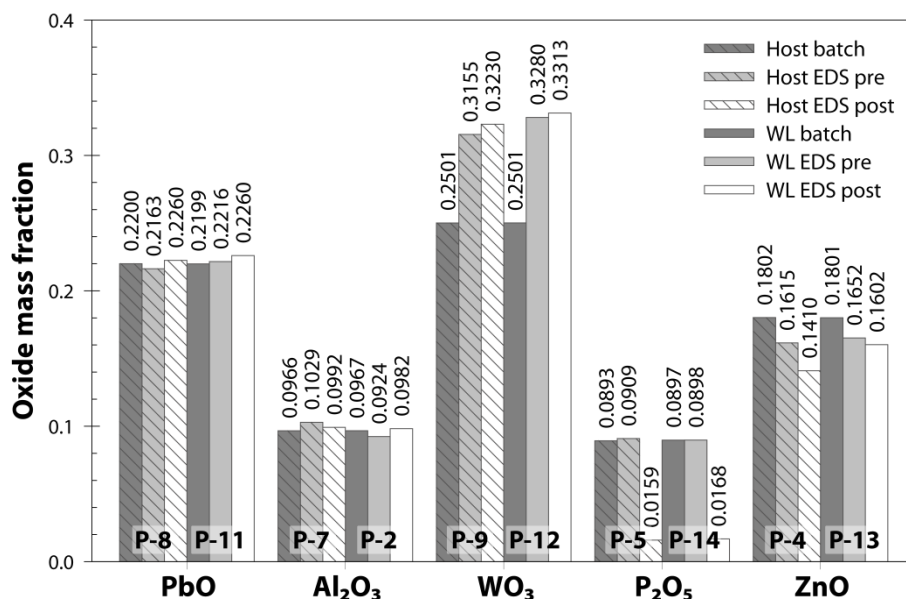
Figure 4.4. Mass fraction of oxide glass additive, normalized without chlorides, as determined using SEM/EDS. The balance for each value is TeO_2 except for the Al_2O_3-B_2O_3 where the B_2O_3 was normalized out since the EDS system could not detect boron with enough certainty. Here the target compositions are listed as "batch", the pre-PCT values are listed as "EDS pre", and the post-PCT values are listed as "EDS post."

The anomaly of the low EDS-measured P_2O_5 was attributed to preferential leaching of a P_2O_5-rich phase in the P_2O_5 glasses, P-5 and P-14 (without and with XCl_{20}, respectively); the P_2O_5 levels following the PCT were measured at 17.8% and 18.7% of the original mass of P_2O_5, respectively. The PbO and Al_2O_3/B_2O_3 glasses showed very congruent data before and after PCT.

The ZnO glasses are similar to the P_2O_5 in that they leached very heavily during the PCT, and the drop in values following the PCT are, again, possibly attributed to a preferential leaching of a ZnO-rich phase in the glasses even though no phase separation was observed in the glasses as-poured. Another possibility is that the low-pH environment accelerated the leaching of these glasses as was observed by Redman and Chen (see Section A-4).[25]

Figure 4.5 shows the measured composition of chloride (by EDS) of the five XCl_{20}-loaded tellurite glasses analyzed by the PCT, before and after the PCT, as compared to the targeted compositions. This separates the glasses into different categories of chloride retention: high ($\geq 90\%$), moderate ($\geq 75\%$), moderate-low ($< 75\%$), low ($< 50\%$). The chloride retention values before and after PCT are presented below:

- Before PCT:
  - High retention: ZnO (**P-13**, 94%), PbO (**P-11**, 90%)
  - Moderate retention: Al_2O_3+B_2O_3 (**P-2**, 83%), WO_3 (**P-12**, 79%)
  - Low retention: P_2O_5 (**P-14**, 37%)
- After PCT:
  - Moderate retention: PbO (**P-11**, 82%)
  - Moderate-low retention: Al_2O_3+B_2O_3 (**P-2**, 63%), WO_3 (**P-12**, 59%)
  - Low retention: ZnO (**P-13**, 22%), P_2O_5 (**P-14**, 1.5%)

It is worth noting that the measured chloride values are close to the targeted values in most of the glasses, although due to the poor durability of the P_2O_5 and ZnO glasses, these values were quite low in the

measured compared to the targeted values. In all of the systems, a larger discrepancy from the targeted value was measured for chloride in the post-PCT sample.
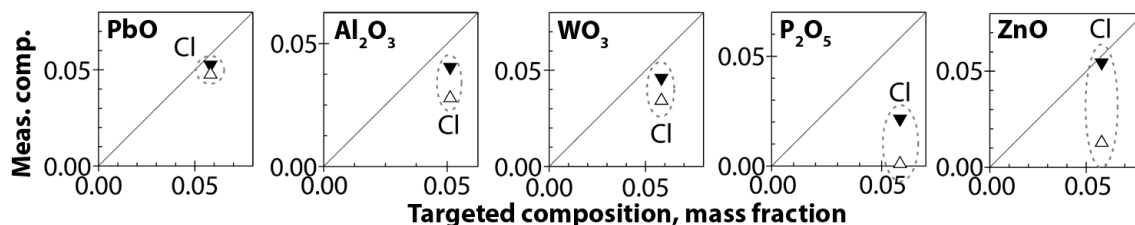

Figure 4.5. Measured (by EDS) versus targeted mass fraction of chloride in the five $X\text{Cl}_{20}$-loaded tellurite glasses analyzed by the PCT. Upside down, closed triangles represent the measured values from the pre-PCT glasses and the upright, open triangles represent the measured values from the post-PCT glasses.

A more detailed description of EDS data comparisons can be found in Appendix D, where the compositions of all ten PCT glasses before and after PCT are listed in mass% for TeO_2, K, Cl and primary glass additive.

4.3.3   Tellurite Glasses: X-Ray Diffraction

All of the glasses used for PCT were analyzed using XRD before and after PCT in the form of fine powders to reduce preferred-orientation effects. Some of the scoping and post-PCT batches were also analyzed by XRD. Before PCT, all ten of the PCT glasses were determined to be amorphous (see Figure 4.13, Figure 4.20, Figure 4.24, Figure 4.29, and Figure 4.33). Figure 4.6 shows fitted backgrounds for the amorphous pre-PCT XRD spectra, which show the differences in peak location and intensity. The PbO-glasses show the largest peak intensity suggesting that they are the most structured of the glasses.

Simulated amorphous diffraction patterns were generated for the three TeO_2 structures (PDF#'s 74-1131, 42-1365, 78-1713) that matched diffraction peaks for the various glasses; simulations were performed using Jade[®] 6 software with a set crystallite size of 10 nm and are presented at the bottom of Figure 4.6. Many differences are apparent in the simulated amorphous patterns, including the location and intensity of the amorphous humps. It is apparent from Figure 4.6 that some of the glasses seem to fit the simulated orthorhombic TeO_2 phase (74-1131), i.e., $\text{Al}_2\text{O}_3/\text{B}_2\text{O}_3$ glasses, while the other glasses seemed to fit with the tetragonal phases (42-1365 and 78-1713).

It should be noted that of the glasses which crystallized TeO_2 phases during the PCT (i.e., P-7, P2, P-5, P-14, P-4, and P-13), those containing $X\text{Cl}_{20}$ always formed orthorhombic TeO_2 and those without $X\text{Cl}_{20}$ always formed tetrahedral TeO_2. This demonstrates that mixed-chloride additions to the tellurite glass network affect the structure of the network in a consistent way.
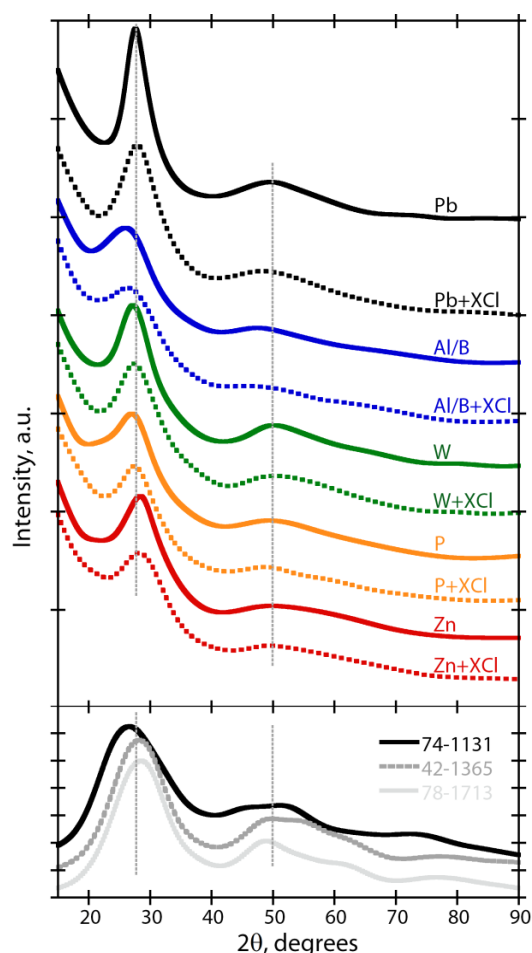
Figure 4.6. XRD summary plot showing the amorphous background fits for all glasses before PCT for comparison with three amorphous simulated patterns for TeO_2 PDF structures (see Table 4.6). Vertical dotted lines are added as a visual guide for the location of the primary amorphous humps. Spectra are offset to accentuate the differences; although the vertical scale is in arbitrary units, the differential intensities remain unchanged from the original spectra.

Table 4.6. Summary of phases identified in the tellurite glasses. The table shows the PDF and/or ICSD identifications, SG, lattice ("Tetr.", "F-C cub.", "B-C orth", and "B-C monocl." denote tetragonal, face-centered cubic, base-centered orthorhombic, and base-centered monoclinic, respectively), unit cell dimensions, and the references for the patterns. See Table 4.3 for more information.

Phase ID	PDF#, ICSD#	SG	Lattice	Dimensions (a, b, c)	Reference
TeO_2	42-1365, 27515	P41212 (92)	Tetr.	4.810, 4.810, 7.612	Blanchard*
TeO_2	78-1713, 62897	P43212 (96)	Tetr.	4.810, 4.810, 7.613	Kondratyuk et al.[26]
TeO_2	74-1131, 26844	Pbca (61)	Orth.	12.04, 5.464, 5.607	Beyer et al.[27]
$Pb_2Te_3O_7$	43-0549, N/A	Fm-3m (225)	F-C cub.	5.647, 5.647, 5.647	Kulcu[28]
$Na_2Te_2O_7$	35-1263, N/A	Imm2 (44)	B-C orth.	7.233, 10.10, 7.454	Knop & Demazeau[29]
Ba_3WO_6	33-0182, N/A	Fm-3m (225)	F-C cub.	17.18, 17.18, 17.18	NBS**
$Zn_2Te_3O_8$	89-4454, 50705	C2/c (15)	B-C monocl.	12.68, 5.200, 11.79	Feger et al.[30]

*Blanchard, F., Department of Geology, University of Florida, Gainesville (1990).

National Bureau of Standards (U.S.) Monogr. 25, **19, p 21 (1982).

4.3.4   Tellurite Glasses: Product Consistency Test

Figure 4.7 shows the average normalized release for Na and Cl, NL_{Na} and NL_{Cl}, respectively. The criterion for direct comparison between the chemical durabilities of the standard reference materials and the waste-loaded glasses fabricated in this study is the normalized release of sodium (NL_{Na}).

Generally, in order to be considered an acceptable waste form, the waste form should be more durable than the EA glass.[10] For the LRM tested in this study, NL_{Na} was 0.504 ± 0.014 g/m². According to the results presented in Figure 4.7, glasses P-13 and P-14 are disqualified as candidate waste forms due to NL_{Na} exceeding that of the EA glass. P-11 was comparable to the LRM reference in chemical durability with a NL_{Na} value of 0.478 compared to the LRM value of (0.509 ± 0.59 g/m²).[18] The values across the five candidate glasses that were tested with XCl_{20} were more variable than expected, ranging from 0.478–88.9 g/m², with the high bound being the ZnO glass with chlorides (P-13).

It is also worth noting that the NL_{Cl} is not congruent with the NL_{Na}. The general trend is $NL_{Na} > NL_{Cl}$, though this is not the case with P-11. The Al_2O_3-B_2O_3 and WO_3 glasses demonstrated low-to-moderate NL_{Na} release rates with values near the EA glass. The full set of NL_i values (measured by ICP-OES and IC) for all ten PCT tellurite glasses are listed in Appendix C.
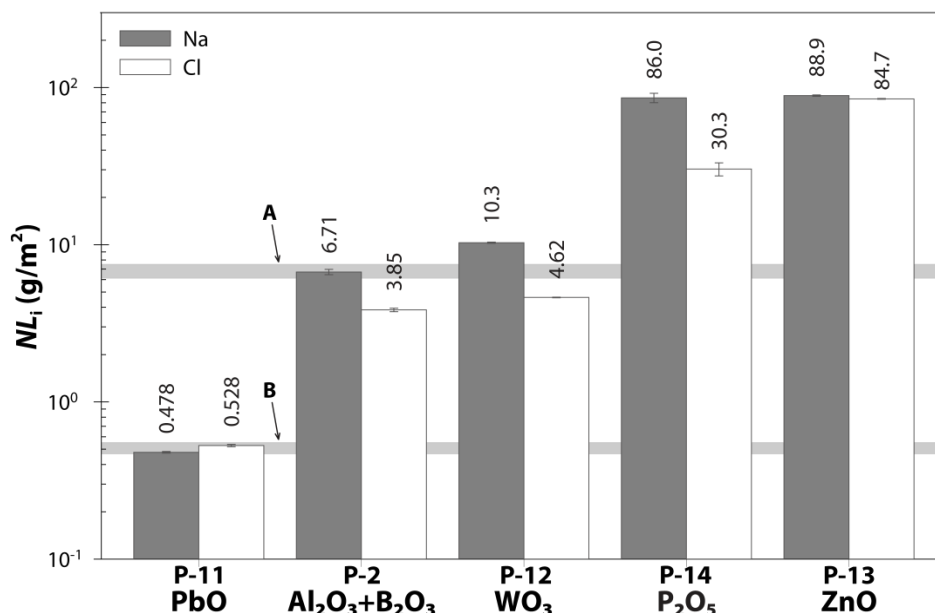

Figure 4.7. Average normalized release NL_i (i = Na, Cl), g/m², calculated from ICP-OES analysis, from waste-loaded glasses. Order of glass families was arranged from the most durable on the left to the least durable on the right. NL_i values from the waste-loaded glasses are categorized above according to the secondary glass components. The horizontal gray regions labeled **A** and **B** are the ranges of NL_{Na} for the Environmental Assessment (EA) glass reference material[10] (6.81 ± 0.95 g/m²) and the LRM reference material[18] (0.509 ± 0.59 g/m²), respectively.

The pH values of the leachates were compared between the host and waste-loaded glasses, and this data is presented in Figure 4.8. As seen in Figure 4.8, the pH varied significantly among the ten different glasses (from 2.04 in the host P_2O_5 glass (P-5) to 6.15 in the WO_3 glass with chlorides (P-12). With the exception of the Al/B glass, all of the waste-loaded glasses showed a pH increase over the host glasses. The low pH values observed for the P_2O_5 glasses (P-5 and P-14) were attributed to a preferential loss of P_2O_5 (in the form of PO_4^{3-}) into the leachate accounting for a low measured mass fraction of P_2O_5 in the post-PCT glasses. This suggests that the P_2O_5 glasses were possibly phase separated and a high-P_2O_5 phase leached out preferentially.
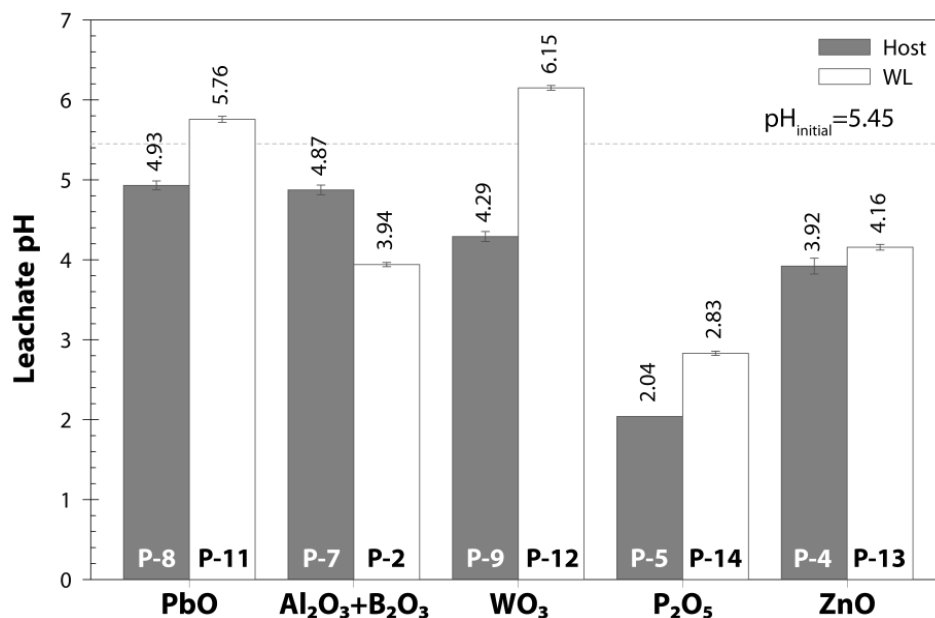
Figure 4.8. The average leachate pH measured post-PCT for all glasses. The initial leachate pH (5.45) is represented by the dotted gray line.

The results from the ICP-MS analysis suggest that samples were mishandled during processing; hence, that data was not used to draw conclusions from the PCT.

4.3.5   Tellurite Glasses: Detailed Discussions of Individual Systems

4.3.5.1 TeO_2-B_2O_3 System

Two scoping tests in the TeO_2-B_2O_3-XCl_{20} system were performed to provide a comparison between the batching methods of the present study and those of the FY2009 study. Each batch had a nominal composition of 85 mass% TeO_2, 5 mass% B_2O_3, and 10 mass% XCl_{20} and was melted at 725°C for 30 minutes. The glasses produced were phase separated (> 50% second phase) and differed in color from the FY2009 glasses. Due to phase separation and inconsistency with previous batches in the FY2009 tests, this glass system received no further consideration.[1]

4.3.5.2 TeO_2-PbO System

Five scoping tests were performed with baseline binary compositions melted at temperatures between 830–980°C. Volatilization was readily visible after removing the crucible lid, and in rare cases the glass product contained traces of a reduced metal phase. Stanworth[15] only reported a melting temperature of 950°C without mention of the length of heat treatment necessary to melt the glass, and additional references were consulted only after several additional high-temperature tests were completed with unsatisfactory results.

Several studies report the dissolution of ceramic crucible materials (silica, alumina and zirconia) in tellurite glass systems. Stanworth[15] reported silica miscibility in TeO_2-PbO melts where two 10 g batches of 15 and 30 mass% PbO devitrified slightly upon cooling, but the addition of 4 mass% silica yielded clear glass. Four scoping tests investigated the glass-forming ability of TeO_2-PbO glasses with small additions of SiO_2. Two batches with addition of 4 mass% SiO_2 were melted at 800 and 950°C, and two tests with a 1 mass% SiO_2 addition were melted at 800°C. All were unsuccessful in making clear (i.e., single phase) glass. Figure 4.9 is a representative picture (of S-5) that illustrates a separated silica-containing phase in TeO_2-PbO glass. In this glass, the undissolved solids (UDS) aggregated into a cap over the molten material in the crucible. Sufficiently high temperatures produced a sintered disc and a glassy material with a metallic appearance, suggesting at least a partial reduction of the oxide to a metal.

Figure 4.9. Glass S-5. The glass that formed is opaque and cream-colored, and most of the silica was not incorporated into the melt. The diameter of the glass in the picture is ~2 cm.

The batch composition of 78 mass% TeO_2 and 22 mass% PbO was successfully processed at 705°C into glasses S-14 and P-8 for scoping and PCT glasses, respectively. The same composition was then loaded with 10 mass% XCl_{20} and successfully processed at the same melting temperature to product P-11. The processing temperature used to melt these four glasses was chosen based on the phase diagram constructed by Marinov *et al*.[31] for the TeO_2-PbO system (see Figure A.3). In quenching S-14 and P-8, no volatilization was visually observed, but a bronze discoloration was found on the crucible lid instead of the silver luster of Pt/10%Rh. Pour viscosity was low (50–100 cP). The glasses were transparent and yellow. An octahedral crystalline phase was found in both glasses (see Figure 4.10) and attributed to $Pb_2Te_3O_7$ (PDF#43-0549) as determined by XRD. Around the perimeter, crystallization was dense with the thick crystal chains (Figure 4.10A), while closer to the center of the glass and the air-exposed surface it was sparse with individual crystals near the edge of the air-exposed surface (Figure 4.10B). A crystal formation observed in P-8 but not in S-14 was a star formation (Figure 4.10C). Each arm of a star formation had a needle-like core (Figure 4.10D).
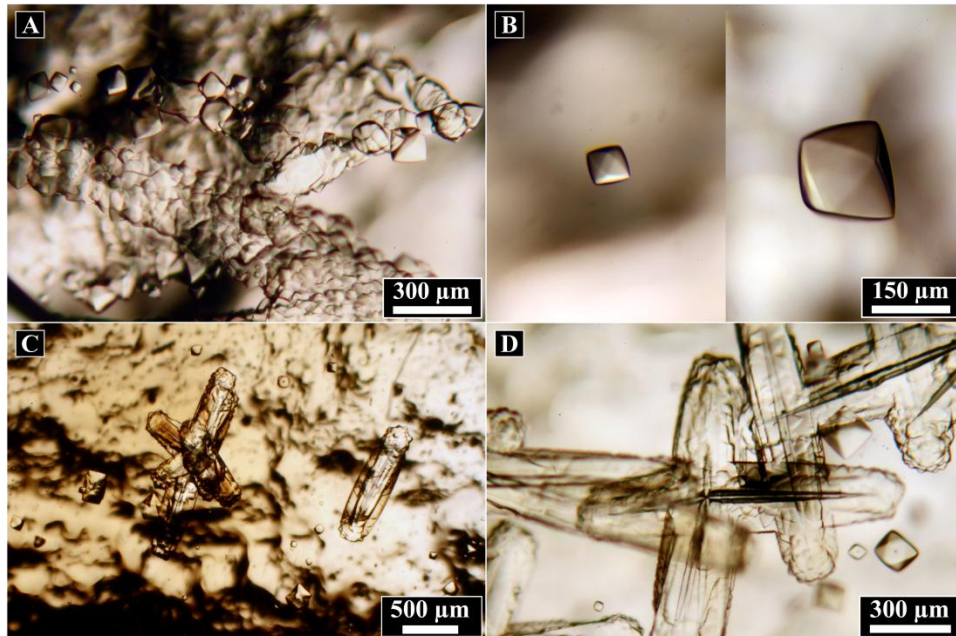
Figure 4.10. Low magnification micrographs of Glasses S-14 (A, B) and P-8 (C, D). (A) Crystal chains around the glass perimeter in S-14, and (B) individual crystals in S-14, also present in P-8. (C) and (D) are low and higher magnification micrographs illustrating the star crystal formation found in P-8 and its features. Also, a very small quantity of a gray crystalline phase was observed on the bottom of P-8.

In the quenching step for glass P-11, a light volatilization was observed and the estimated pour viscosity was low (≤ 10 cP). The glass was orange; under reflected light, polarized spots on the air-exposed surface

were observed. The origin of these small polarized regions is uncertain and warrants further investigation.

The octahedral crystal present in the binary glasses was not found in P-11, but phase separation was present. Undissolved solids and small patches of a thin layer of reduced metal (i.e., black spots) or crystallized salts were observed on the Inconel quench surface. These phases constituted a very small quantity of the entire glass ($\lesssim 0.1$ mass%). The glasses used for PCT had a very uniform appearance (see Figure 4.11) and the -100/+200 mesh size fraction looked very similar in the glasses before and after PCT (Figure 4.12).
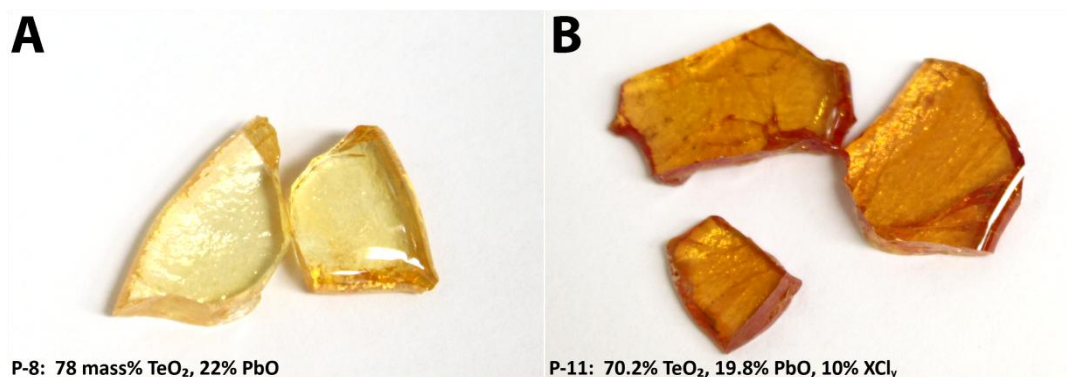
Figure 4.11: Glasses (A) P-8 and (B) P-11 with compositions (in mass%) listed on the images.
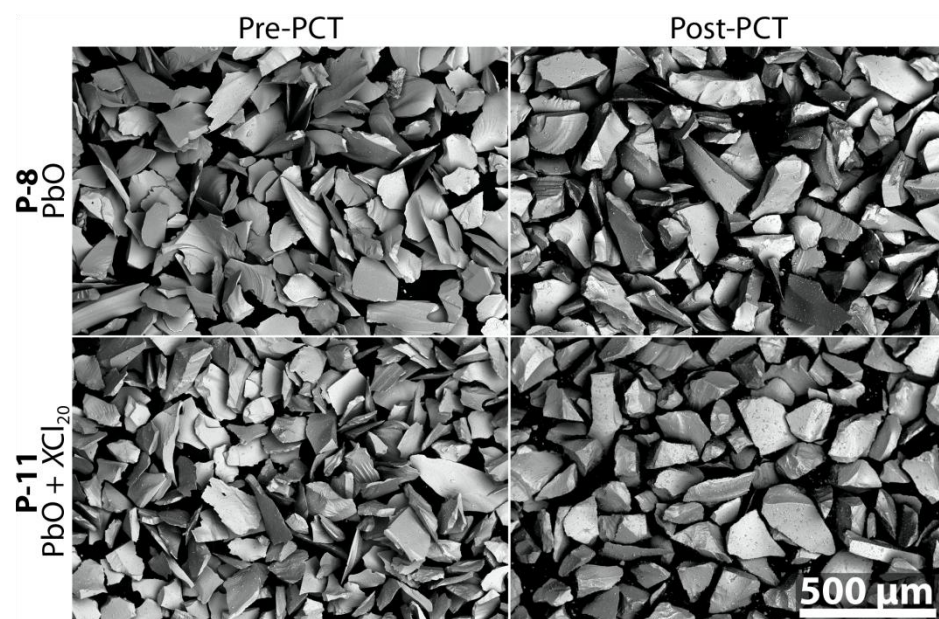
Figure 4.12. SEM micrographs of the PbO glasses P-8 and P-11 before and after PCT. All particles analyzed were -100/+200 mesh.

The XRD spectra of the PbO PCT glasses P-8 and P-11 (without and with XCl_{20}, respectively) reveal that the glasses did not crystallize much during the PCT; see Figure 4.13. A very small amount of $Pb_2Te_3O_7$ was observed in P-8 following the PCT.

Figure 4.13. XRD patterns for the lead glasses with and without XCl_{20} before and after PCT. The circles on the pattern show the locations of the diffraction peaks which were identified as the phase $Pb_2Te_3O_7$ (PDF#43-0549).
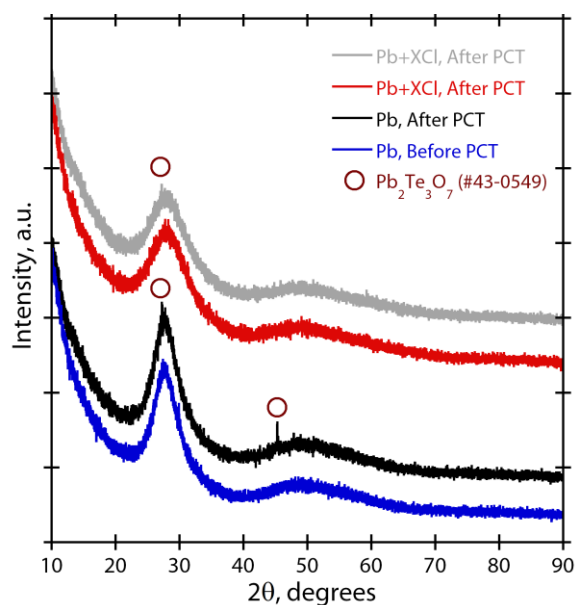
It is also worth noting that the NL_{Pb} values for the P-8 and P-11 in the PCT were well below that measured for the LRM glass as depicted by Figure 4.14 and thus are off the chart.
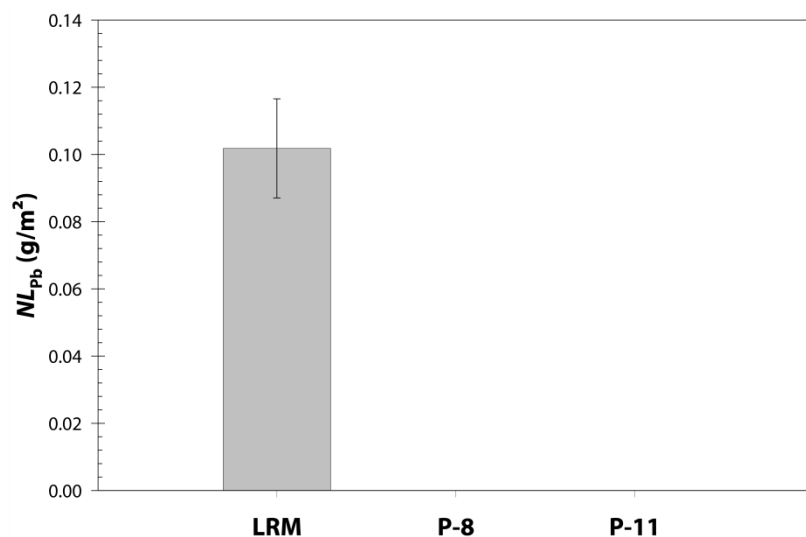
Figure 4.14. Plot showing NL_{Pb} measured in the LRM glass in comparison to the P-8 and P-11, the lead glasses with and without the chlorides, for which the NL_{Pb} was below detection limit.

INCREASED WASTE LOADING PbO GLASS FABRICATION

An additional batch experiment with 78 mass% TeO_2, 22 mass% PbO composition was performed after the PCTs to explore its waste-loading capacity. Here, a glass with 15 mass% XCl_{20} was batched and processed in the same fashion as with P-11. The result was a glass that had a two apparent phases (Figure 4.15). The specimen was found XRD amorphous suggesting a possible immiscible liquid phase separation. Through SEM-EDS analysis, the top phase in Figure 4.15-B was determined to be higher in chloride (by 36%), sodium (by 23%), potassium (by 50%), and lead (by 9%) than the transparent, red

phase with the balance in the red phase being a higher quantity of measured tellurium. Further investigation will be performed on this system to explore the waste loading capacity.

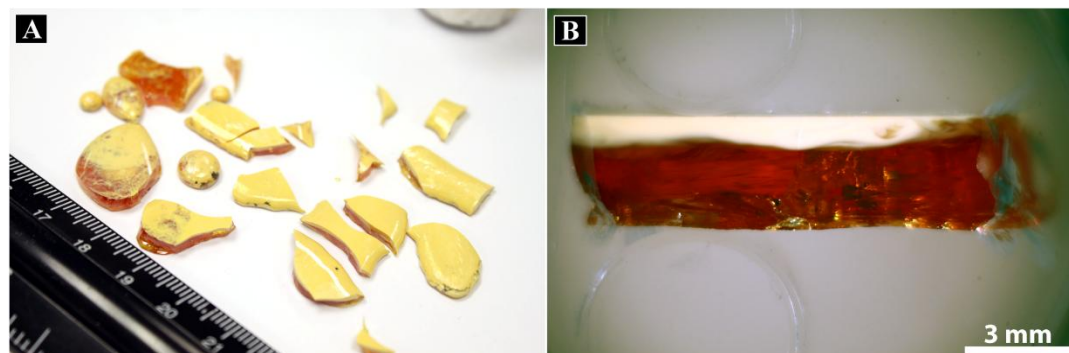Figure 4.15. (A) Optical photograph and (B) micrograph of the 15 mass% XCl_{20}-loaded lead glass (66.3 mass% TeO_2, 18.7 mass% PbO balance) showing the two-phase immiscibility.

4.3.5.3   TeO$_2$-Al$_2$O$_3$-B$_2$O$_3$ System

A batch composition of 82.2 mass% TeO_2, 8.8 mass% Al_2O_3 and 9.0 mass% B_2O_3 (see Section A-5.2) was successfully processed at 830°C to produce glass S-6. The alumina source was a coarse high-purity powder (described in Appendix B as PNNL 118316). No volatilization was visually observed when the lid was removed prior to quenching on the Inconel plate. The pour was relatively viscous (100–200 cP). Glass S-6 was transparent and colorless, and it appeared to be a good candidate for further analysis. Volatilization at 830°C was found to be high for subsequent chloride-loaded ST glasses. Lower processing temperatures were tested, and 730°C was deemed satisfactory to form a glass while reducing volatilization.

Glass P-0 was produced after melting a 20 g batch of 8.8 mass% Al_2O_3 and 9 mass% B_2O_3 at 730°C. P-0 was similar to S-6, but white UDS, likely undissolved alumina, were readily visible on its air-exposed surface. After examining S-6 again, UDS were also found at its air-exposed surface. Closer examination was conducted using optical microscopy (see Figure 4.16). A precipitated crystal phase and UDS were observed, estimated to constitute ≲ 1 volume % of the glass (see Figure 4.16).
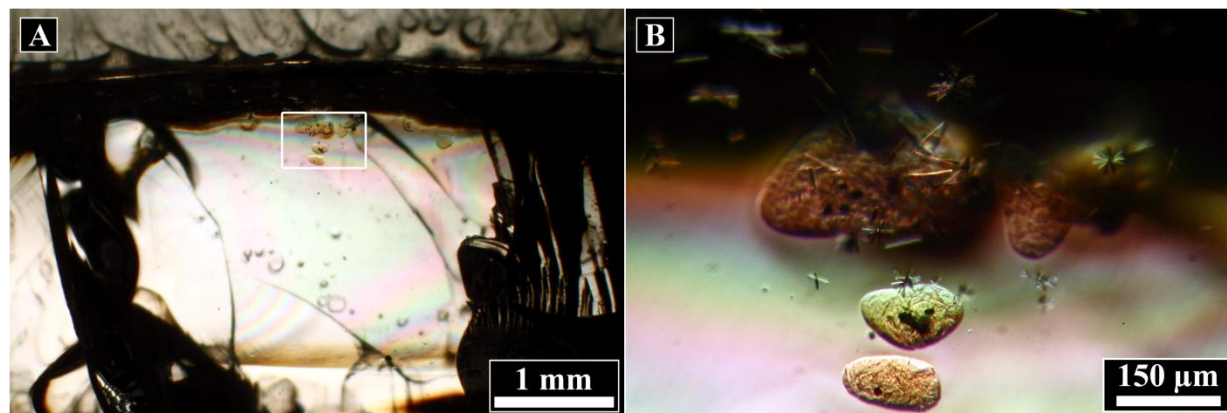
Figure 4.16. Cross-sectional optical micrographs of the center of S-6. (A) This low magnification micrograph depicts the bulk of the glass, which is optically transparent and appears amorphous. Crystals and undissolved particles are present close to the air-exposed surface of the glass. The bubbles in the lower half of the glass are in the adhesive between the thin section and the substrate. (B) A higher magnification micrograph of the region surrounded by a square in (A) shows the features of the crystal phase and the undissolved particles.

An additional scoping test was performed with -325 mesh Al_2O_3 (described in Appendix B as PNNL 67135) and melted at 730°C. It was hoped that finer particles of alumna would enter the glass matrix more readily than the coarser alumina. No volatilization of components was observed. The glass S-23 was transparent and pale green in color. Optical microscopy showed a negligible fraction of undissolved particles. Crystallization was not observed in S-23 as it had been in glass S-6.

Two more PCT-scale glasses, P-2 and P-7, were batched with the -325 mesh alumina and melted at 693°C and 720°C, respectively. *Glass P-2 was batched with a miscalculated composition of salts based on incorrect loss on drying (LOD) values to the additives.* The difference between the XCl_{20} and the mixed chlorides used for this glass, XCl_y, can be found in Appendix E. It was significantly phase separated, with varying color and UDS observed under the microscope. Glass P-7 was similar to S-23, i.e. a pale green transparent glass. Figure 4.17 shows low-magnification micrographs of glasses P-7 (Figure 4.17A) and P-2 (Figure 4.17B), showing the UDS present in both, and the phase separation representative pieces of the two glasses side by side for visual comparison. In spite of the non-ideal processing conditions and quality of the glasses, it was decided that they would still undergo PCT for comparison.

P-7: 82.2 mass% TeO$_2$, 8.8% Al$_2$O$_3$, 9% B$_2$O$_3$ P-2: 74% TeO$_2$, 7.9% Al$_2$O$_3$, 8.1% B$_2$O$_3$, 10% XCl$_y$
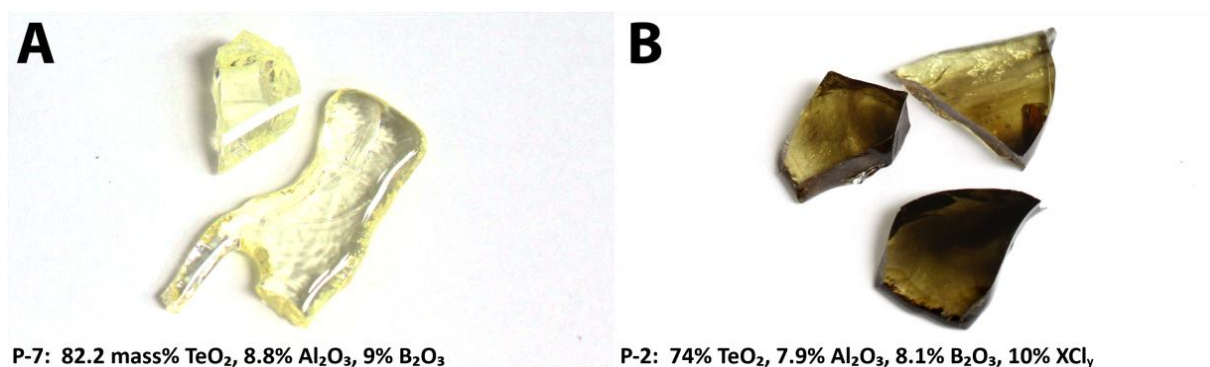
Figure 4.17. PCT glasses (A) P-7 and (B) P-2 labeled with their batch compositions in mass%.

Both P-7 and P-2 glasses had undissolved materials present prior to PCT, though the quantities were below XRD detection limits. Figure 4.18 shows a few of the high-density regions where these undissolved materials were observed. The glasses did not appear to change much before and after the PCT (see Figure 4.19), though both glasses will be analyzed further using SEM-EDS to look for compositional gradients considering that these glasses both crystallized heavily during the PCT.

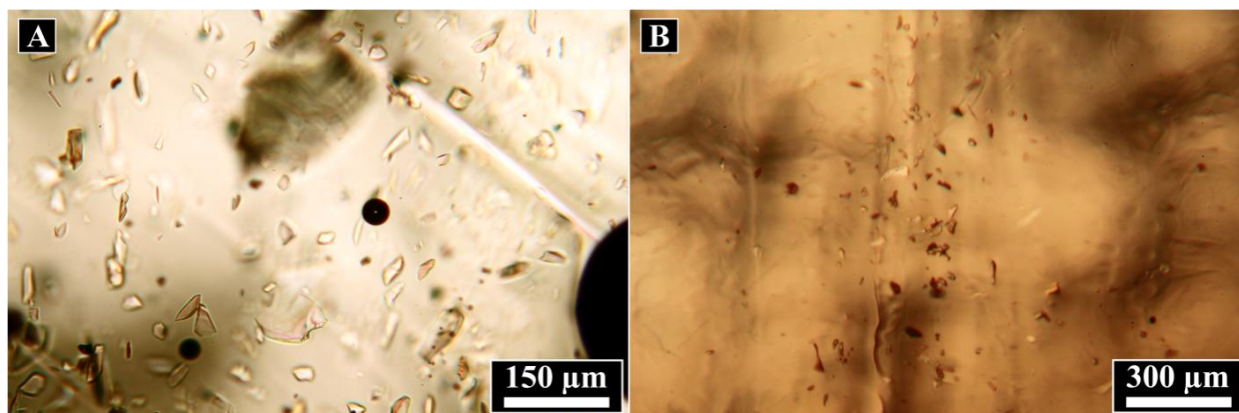

Figure 4.18. (A) PCT glass P-7 and (B) PCT glass P-2 showing undissolved material in the glasses.

The PCT glasses appeared visually similar to post-PCT as pre-PCT (Figure 4.19), and the NL_{Na} and NL_{Cl} releases were low (Table 4.5, Figure 4.7). Orthorhombic TeO_2 crystalline phases were observed in the post-PCT sample but not in the pre-PCT sample (see Figure 4.19 and Figure 4.20).
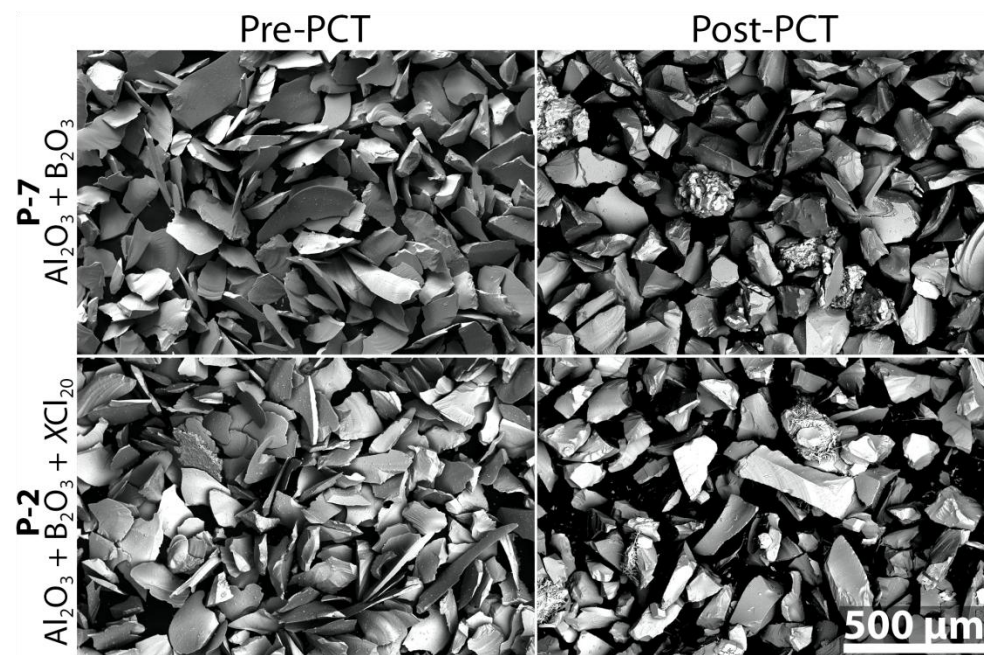
Figure 4.19. SEM micrographs of the Al_2O_3/B_2O_3 glasses P-2 and P-7 before and after PCT. All particles analyzed were -100/+200 mesh.

Figure 4.20. XRD patterns for the Al-B glasses with and without XCl_{20} before and after PCT. The symbols on the pattern show the location of the diffraction peaks: the closed circles represent a tetragonal TeO_2 phase (PDF#78-1713), the closed squares represent an orthorhombic TeO_2 phase (PDF#74-1131), and the open squares represent an orthorhombic alkali tellurium oxide phase ($Na_2Te_2O_7$, PDF#35-1263).

4.3.5.4   TeO$_2$-WO$_3$ System

The scoping test performed in the TeO_2-WO_3 system involved melting a host composition of 75 mass% TeO_2 and 25 mass% WO_3 at 700°C. No volatilization was visually observed, and the melt pour had a low viscosity (50 cP). Undissolved solids were present in the residual glass material in the crucible after pouring, around the top of the melt meniscus (Figure 4.21A). The glass that poured and quenched was a brilliant yellow color (Figure 4.21B). Glass S-27 was placed back into the crucible and re-melted at

725°C to attempt to reconstitute the undissolved materials from the first melt. The glass product after this heat treatment was a transparent green color with estimated phase separation of < 0.1 mass% (see Figure 4.21C); at higher magnification, the phase appears to be refractory UDS (see Figure 4.21D).

Figure 4.21. Glass S-27. (A) Undissolved materials were present close to the melt meniscus after the first melt. (B) Amorphous glass after first melt. (C) Amorphous glass after second melt. (D) Undissolved materials in the glass after second melt.

The same composition was scaled up to process the baseline glass P-9 and the waste-loaded glass P-12 with 10 mass% XCl_{20}. P-9 was melted at 700°C for 28 minutes and then at 725°C for 30 minutes. The pour viscosity was estimated visually to be 100 cP. The glass varied slightly in color, mostly yellow with a small fraction of orange. A small fraction of undissolved materials (< 1 mass%) was left in the residual glass that did not pour out of the crucible. The glass that did pour was observed under the microscope to contain a small percentage of what appeared to be undissolved materials.

Glasses P-10 and P-12 were processed with the same baseline composition (75 mass% TeO_2 and 25 mass% WO_3) loaded with 10 mass% XCl_{20}. P-10 was melted at 725°C and exhibited the worst case of volatilization observed overall. An off-gas was flowing out of the crucible from under the lid prior to pouring. The off-gas was so thick that the melt was difficult to see and continued to flow from the melt vigorously after pouring onto the Inconel quench plate. The residue that formed on the quench plate was among the most severe of the tellurite glasses in this study. A film of red beads formed on the lid during the melting process, and what appeared to be UDS and glass spanned ~1 cm down the outside of the crucible. The viscosity of the melt was low (~10 cP). In order to decrease the volatilization, P-12 was processed at 675°C. The pour viscosity was similar. The volatilization and the residue were both still among the most extreme cases observed during waste-loaded glass processing.

As seen in Figure 4.22, the PCT glasses had a very uniform appearance; however, a color gradient was present in P-12, varying from orange at the beginning of the pour to a darker orange-red at the end of the pour. This color gradient can be observed partially in Figure 4.22-B. The glasses looked very similar before and after the PCT as shown in Figure 4.23.

P-9: 75 mass% TeO_2, 25% WO_3 P-12: 67.5% TeO_2, 22.5% WO_3, 10% XCl_y
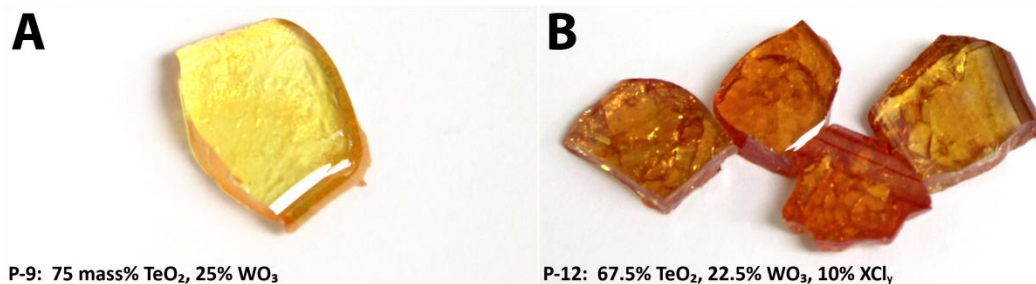
Figure 4.22. PCT glasses (A) P-9 and (B) P-12 with compositions (in mass%) listed on the images.
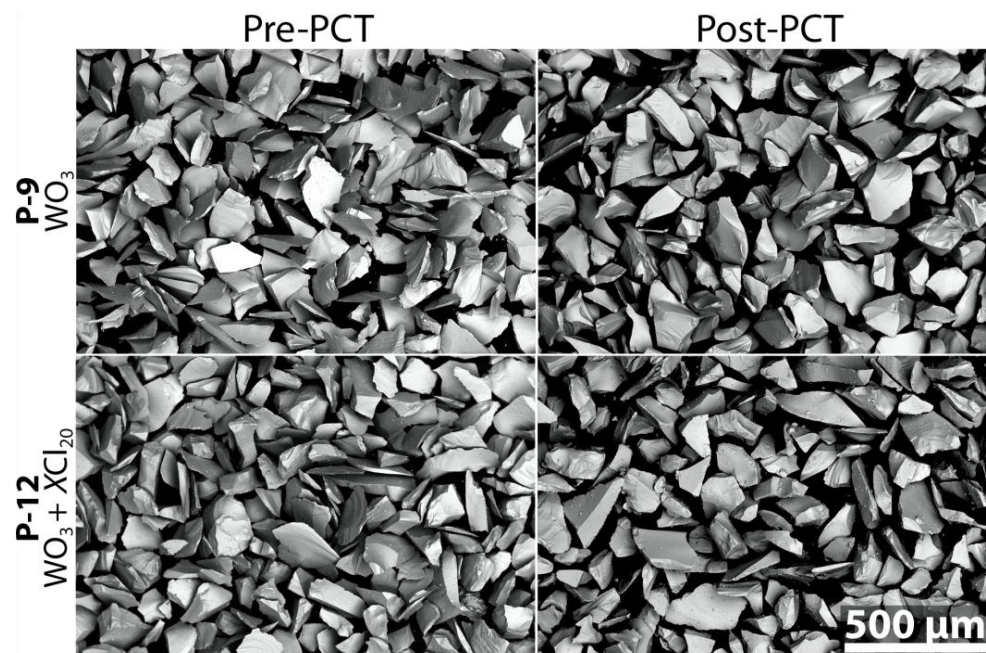
Figure 4.23. SEM micrographs of the WO_3 glasses P-8 and P-11 before and after PCT. All particles analyzed were -100/+200 mesh.

The PCT responses of glasses P-9 and P-12 were relatively low as seen in Figure 4.7. A small amount of Ba_3WO_6 (PDF#33-0182) was observed following the PCT of P-12 as seen in Figure 4.24.
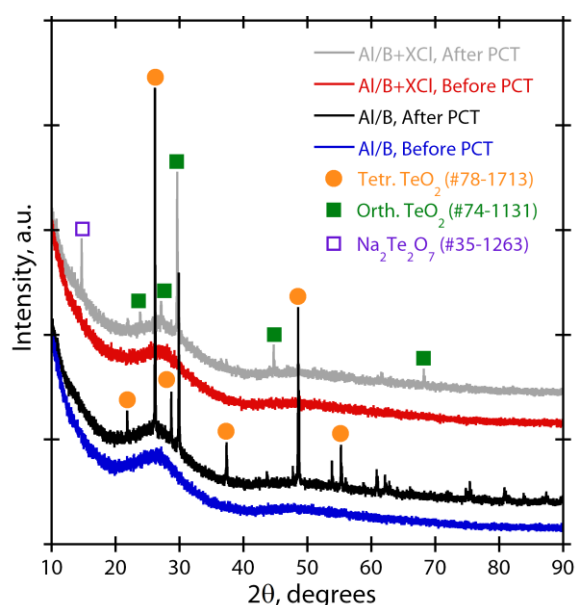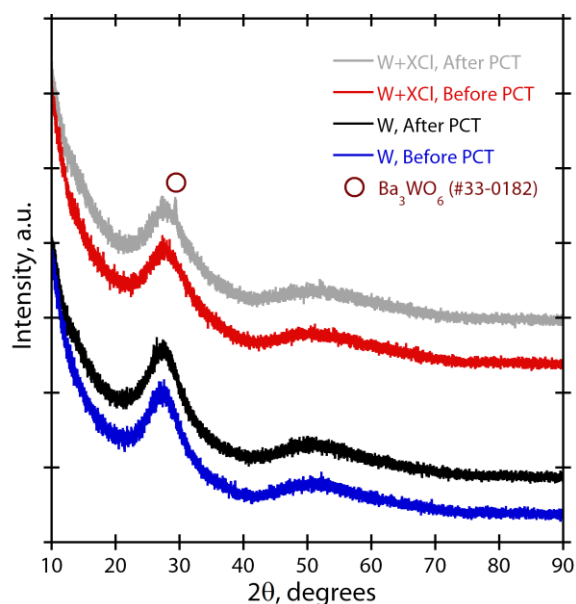

Figure 4.24. XRD patterns for the WO_3 glasses with and without XCl_{20} before and after PCT. The symbol on the pattern shows the location of the diffraction peak which was identified as the phase Ba_3WO_6 (PDF#33-0182).

4.3.5.5   *TeO_2-P_2O_5 System*

Glasses within this system were difficult to batch on account of the hygroscopic nature of P_2O_5. As soon as the powder was removed from the glass scintillation vial, it absorbed water, turning sticky. An interesting phenomenon was observed during the batching process: when the measured powders were

mixed in the agate mortar and pestle, the mixture turned from white to bright yellow with the addition of P_2O_5.

The first scoping glass of this system, S-22, was batched at the nominal batch composition of 90 mass% TeO_2 and 10 mass% P_2O_5. Volatilization was not observed upon removing the lid from the crucible during a 700°C heat treatment. The viscosity of the pour was estimated to be 300–400 cP. The glass was transparent, yellow, and virtually amorphous. No phase separation was found upon closer inspection under an optical light microscope, but a significant number of bubbles were present in the melt.

The next scoping glass, S-24, was the same baseline composition batched with 10 mass% XCl_{20}. It was melted in three 30-minute heat treatments at ~600, 700 and 800°C, respectively, to determine an appropriate melting temperature for the waste-loaded glass. S-24 was poured, quenched, and placed back into the crucible without grinding. After each heat treatment, the glass was opaque. After the 600°C heat treatment, the glass was white, highly viscous (800 cP), and contained a large fraction of UDS. No volatilization was observed upon removing the lid from the crucible. After the 700°C heat treatment, light volatilization was observed. The pour had an estimated viscosity of 300–400 cP, and the glass was a milky off-white. Most of the UDS entered the melt. The residual glass in the crucible was white, orange, and pink in color (see Figure 4.26, for example). After the 800°C heat treatment, no UDS were observed. Volatilization was heavy, and the viscosity was low (50 cP). The glass was pale orange in color.

Glass S-25 had the same batch composition but was subjected to only one heat treatment, at 800°C. The volatilization was heavy, with fume leaving the melt before and several seconds after pouring. S-25 appeared similar to S-24 after the 800°C heat treatment: an opaque, pale-orange glass. In order to minimize volatilization, a melting temperature of 675°C was chosen.

A second composition was tried, 9 mass% P_2O_5, which is closer to the eutectic composition (8.3 mass% P_2O_5) and the middle of the glass-forming range of the TeO_2-P_2O_5 system; this glass, S-26, was similar to S-22. The batch composition of S-26 was scaled up to 20 g in P-5 and melted at 675°C, yielding a glass with the same results as observed with S-26. After pouring, quenching, and removing residual glass, black spots were present on the crucible wall. Figure 4.25-A and -B show UDS present in P-5 and S-26, respectively. These constituted a negligible fraction of the total amount of glass.
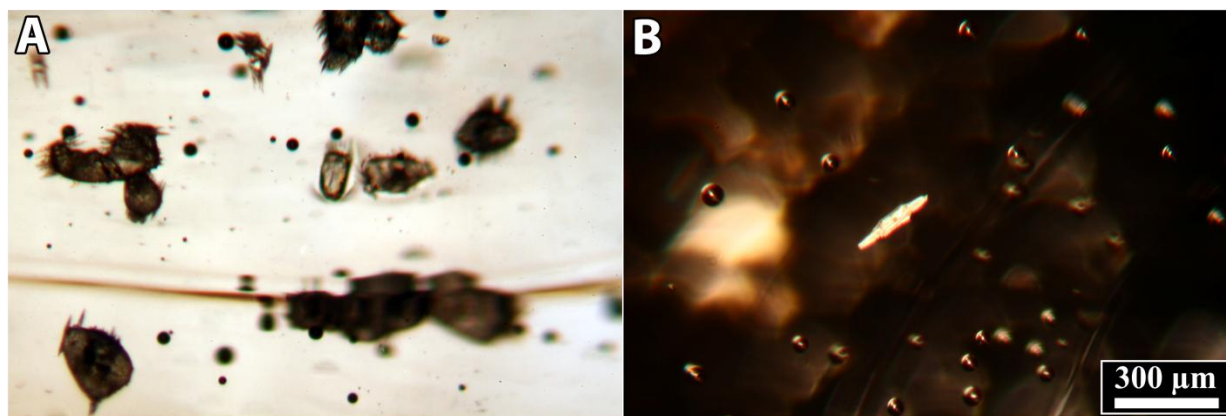
Figure 4.25. Undissolved solids observed in (A) P-5 and (B) S-26. Scale bar applies to both micrographs.

In P-14, the glass was opaque and varied in color from white and orange at the beginning to pink at the end of the pour (see Figure 4.26). In the crucible, the glass that did not pour was white and reddish-pink. The bottom of the crucible was caked with UDS. P-14 was ground in an Angstrom ring pulverizer and remelted at 675°C. The volatilization was again moderate to high. P-14 appeared to be more homogeneous than observed after the first melt, but a gradient in color was still present.

Figure 4.26. Glass P-14 after the first melt at 675°C, showing the phase separation apparent in the color variation. The large chunk in the micrograph is ~3 cm long.

The glasses looked very different after the PCT, as shown in Figure 4.27. P-5 and P-14 glasses had very similar morphology before the PCT (Figure 4.28), but afterwards both were in the form of single porous discs (similar in appearance to those from the ZnO glasses – see Figure 4.31), which broke apart when they were removed from the PCT vessels.

A

B

P-5: 91 mass% TeO_2, 9% P_2O_5

P-14: 81.9% TeO_2, 8.1% P_2O_5, 10% XCl_y
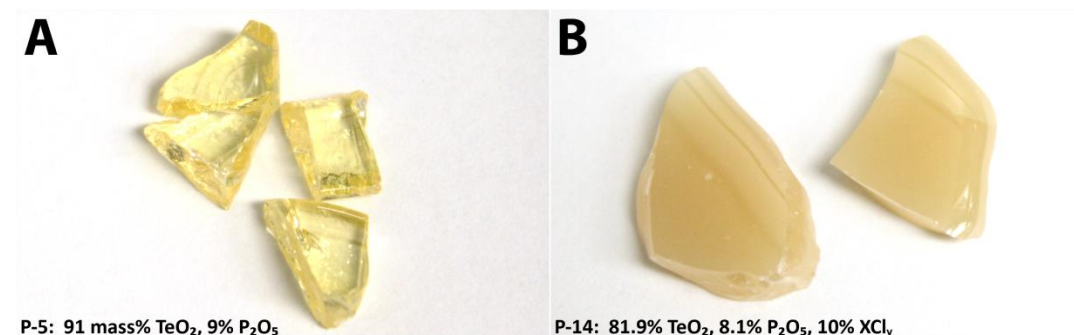
Figure 4.27. Glasses (A) P-5 and (B) P-14 with compositions (in mass%) listed on the images.
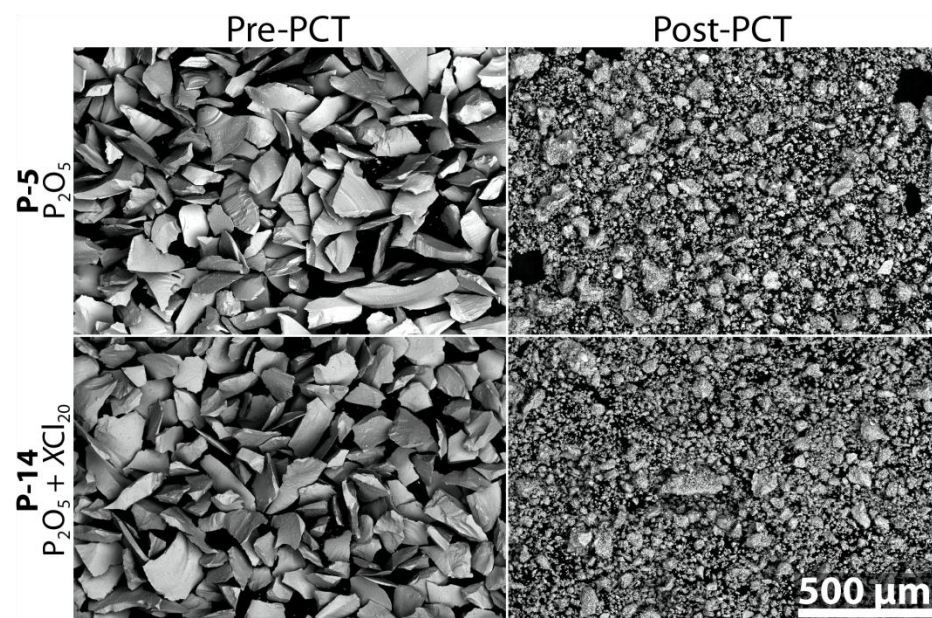
Figure 4.28. SEM micrographs of the P_2O_5 glasses P-5 and P-14 before and after PCT. All particles analyzed before PCT were -100/+200 mesh.

Significant crystallization occurred during the PCT, forming TeO_2 (tetragonal and orthorhombic phases), as shown in Figure 4.29, with very little amorphous phase remaining. As noted previously (see Section 4.3.2), the PCT solution was rich in phosphate relative to the glass composition (Figure 4.4).
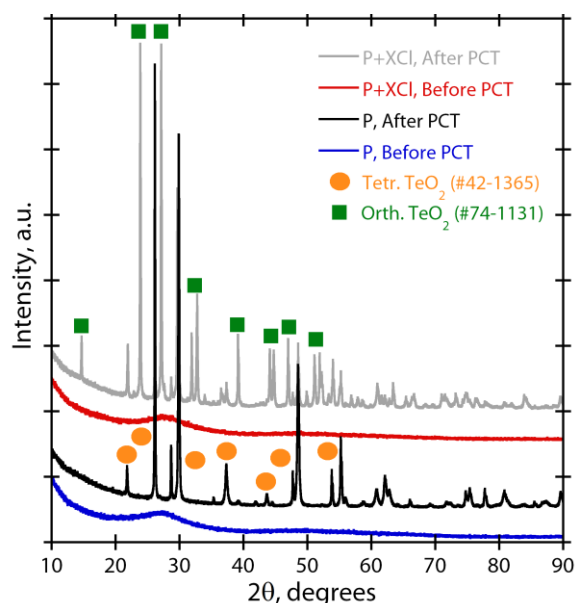
Figure 4.29. XRD patterns for the P_2O_5 glasses with and without XCl_{20} before and after PCT. The symbols on the pattern show the locations of the diffraction peaks: the closed circles identify the tetragonal paratellurite TeO_2 phase (PDF#42-1365), and the closed squares identify an orthorhombic TeO_2 phase (PDF#74-1131).

4.3.5.6   *TeO$_2$-ZnO System*

The host glass composition with 18 mass% ZnO was successfully processed at 730°C to produce glass S-15. No fuming was observed. The pour viscosity was estimated to be around 50 cP. S-15 was a colorless, transparent glass upon cooling. No crystals or UDS were found by light microscopy. The host glass was scaled up and processed at 690°C and quenched on the Inconel. Unlike S-15, P-4 contained UDS first heat treatment at 690°C.

Considering the difference in operating temperatures between the first and second furnaces, P-4 was placed back into the crucible (without milling) and re-melted at 734°C. After quenching, P-4 formed a transparent glass with a very pale yellow-orange color. There were a couple of small pieces of glass with crystallization, which was verified by XRD to be crystalline tetragonal TeO_2 (PDF#78-1713) and monoclinic zincospiroffite, $Zn_2Te_3O_8$ (PDF#89-4454). In contrast with the colorless S-15, P-4 was champagne-colored; see Figure 4.30-A. This could be attributed to the different melting procedure or possibly to the difference in crucible materials. No difference in microstructure was observed.
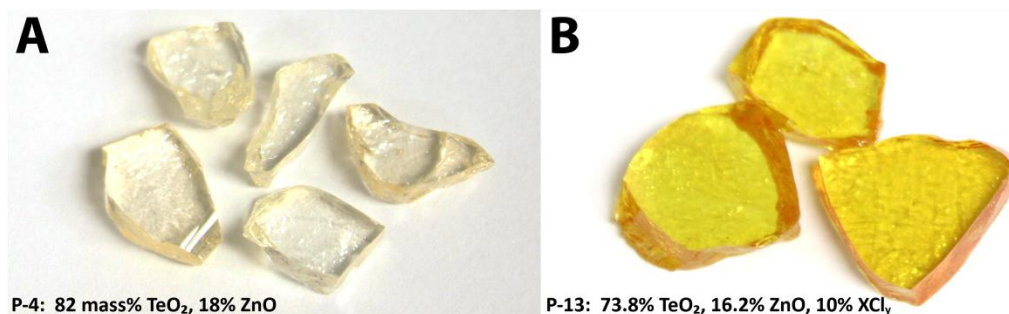
Figure 4.30. Pictures of the ZnO PCT glasses (A) P-4 with no chlorides and (B) P-13 with chlorides. Compositions are listed on the micrographs.

P-13, the glass composition with 18 mass% ZnO and 10 mass% XCl_{20}, was successfully processed at 730°C. The volatilization was low, and the estimated pour viscosity was 10 cP. The glass that formed

was transparent and yellow in the bulk and orange around the edges, as seen in Figure 4.30-B. No crystallization was found in this glass by optical microscopy.

The SEM micrographs of the both glasses at the -100/+200 mesh size fraction before PCT look very uniform and not any different from the rest of the PCT glasses. However, the powders became porous discs during the PCT (see Figure 4.31) and thus were broken into small pieces for the post-PCT SEM/EDS examinations; see Figure 4.32.
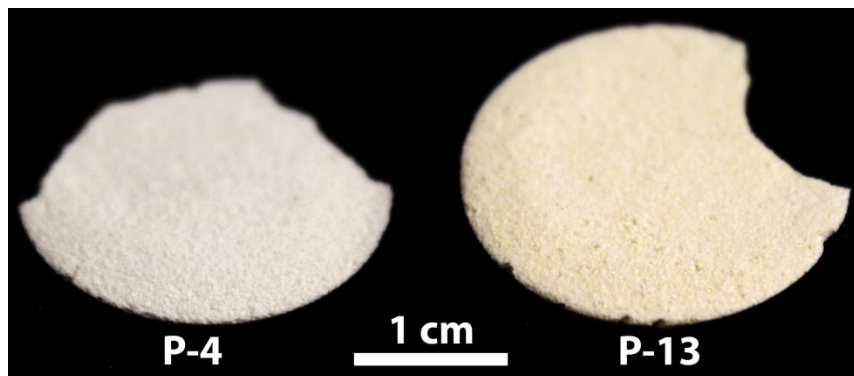
Figure 4.31. Pictures of the porous discs of the ZnO glasses P-4 and P-13 after PCT.
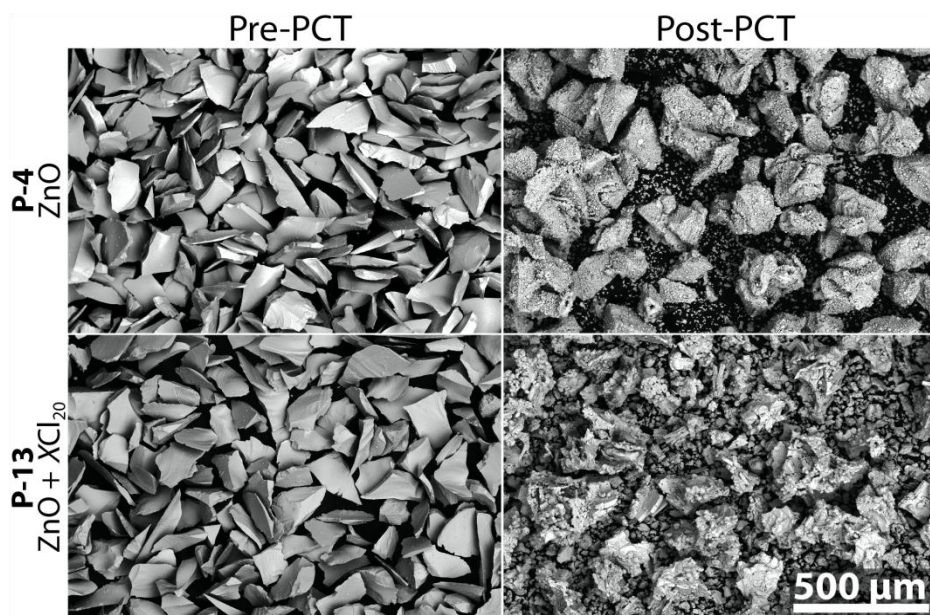
Figure 4.32. SEM micrographs of the ZnO glasses P-4 and P-13 before and after PCT. All particles analyzed were -100/+200 mesh.

X-ray diffraction analyses of P-4 and P-13 revealed that significant amounts of monoclinic $Zn_2Te_3O_8$ (PDF#89-4454), tetragonal TeO_2 (PDF#78-1713), and orthorhombic TeO_2 (PDF#74-1131) formed during the PCT. Although the quantity of $Zn_2Te_3O_8$ was comparable between the two glasses, P-4 showed a much higher quantity of tetragonal TeO_2 than did P-13.
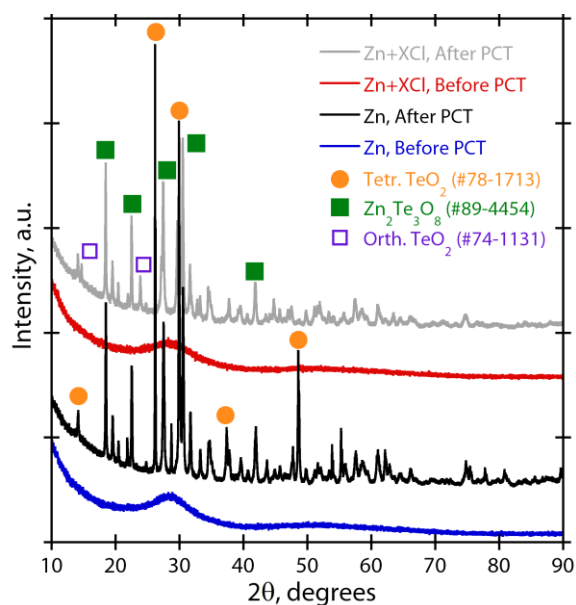
Figure 4.33. XRD patterns for the ZnO glasses with and without XCl$_{20}$ before and after PCT. The symbols on the pattern show the locations of the diffraction peaks. The closed circles represent a tetragonal TeO$_2$ phase (PDF#78-1713), the closed squares represent the monoclinic zincospiroffite, Zn$_2$Te$_3$O$_8$ (PDF#89-4454), and the open squares represent an orthorhombic TeO$_2$ phase (PDF#74-1131).

5.   Conclusions, Future Work, and Process Improvements

5.1   Tellurite Glasses

Five different tellurite glass systems were chosen based on the expanded literature review and were further investigated, including the addition of the following network modifiers/intermediates to TeO$_2$: PbO, Al$_2$O$_3$-B$_2$O$_3$, WO$_3$, P$_2$O$_5$, and ZnO. These glasses had low melting temperatures (675–730°C), low estimated viscosities (~10–400 cP), moderate-to-high densities (4.13–5.16 g/cm^3), and differing PCT NL_{Na} values (0.478–88.9 g/m^2) (see Table 4.5). The high density is important when the waste storage density, or the mass of waste stored in the overall waste form volume, is considered as long as waste loading in not limited by heat. Regarding chemical durability, a few of the glass systems showed promise (i.e., PbO, Al$_2$O$_3$-B$_2$O$_3$, and WO$_3$), and some will not be further pursued (i.e., P$_2$O$_5$ and ZnO).

Future work includes:

- Determine heat-limiting properties of candidate glasses using thermal analysis on candidate glass systems. This includes differential scanning calorimetry (DSC) for T_c, T_g, T_m, T_x, and heat capacity (C_p) as well as and laser flash diffusivity.

- Investigate the Al$_2$O$_3$-B$_2$O$_3$ system further, considering that both the glass with mixed chlorides and the glass without chlorides performed well in the PCT and contain low-cost additives without chemical hazards. Include tests with the XCl$_{20}$ waste addition. To further refine the Al$_2$O$_3$-B$_2$O$_3$ system, different Al$_2$O$_3$:B$_2$O$_3$ compositions will be batched, melted, and analyzed by XRD, OM, and PCT.

- Maximize the waste loading for the TeO$_2$-PbO system. In this work, a waste loading of 15 mass% was demonstrated, though the glass phase separated during quenching and the results are still under investigation.

- Look at other candidate systems, which include the addition of other transition metal oxides, e.g., MoO$_3$,[15] Ta$_2$O$_5$, or Nb$_2$O$_5$.

- Incorporate the Hruby criterion in the glass selections to identify the glass systems with the highest likelihood of success.

- Investigate other chemical durability tests, i.e., single-pass flow-through, etc.

- Perform BET on the particles prior to PCT to determine the exact surface area of the particles.

- Investigate the impacts of slow cooling (e.g., canister centerline cooling) on phase formation and PCT responses.

5.2   Halide Minerals

The sol-gel process proved successful for synthesis of sodalite and, to a limited extent, cancrinite. The sol-gel process produced a fine powder; thus, cold press and sintering was used to consolidate the powder into a waste form package. The most difficult issue associated with the halide mineral waste forms was achieving a bulk density $\geq$ 90% of theoretical, while remaining within the sodalite stability temperature range. NBS-1 glass was added to lower sintering temperature and increase bulk density, with the added benefit of greater stability of sodalite during firing. However, the porosity and surface area still remained higher than ideal. Adding additional NBS-1 glass will address the open porosity, but at the expense of waste loading.

Future work will primarily focus on optimizing waste form consolidation that should translate into reduced surface area. To achieve higher bulk density, the following methods will be evaluated:

- hot isostatic pressing to take advantage of pressure-assisted firing

- additional glass sintering aids to achieve sintering at lower temperatures. A series of glasses will be evaluated versus sintering temperature and bulk density.

- increasing green density, i.e., cold pressing with vacuum and/or vibratory assistance to help consolidate the waste form

- vacuum casting the gel directly prior to drying.

6.   Acknowledgements

7.   References

[1]Crum, J. V., B. J. Riley, S. K. Sundaram, S. A. Arreguin, J. Matyas, M. J. Schweiger, B. T. Rieck, and J. D. Vienna. 2009. *Alternative Waste Forms for Electro-Chemical Salt Waste*. AFCI-WAST-PMO-MI-DV-2009-000293. Pacific Northwest National Laboratory, Richland, WA.

[2]Yoo, T. S., personal correspondence, 2009.

[3]Vienna, J. D., J. Luey, P. R. Hrma, D. E. Smith, R. D. Scheele, H. L. Wigent, and J. V. Crum, "Glass frit development for encapsulation of rocky flats ash,*"* pp. 399-407, *Environmental Issues and Waste Management Technologies in the Ceramic and Nuclear Industries IV*, **93**. Edited by J. C. Marra and G. T. Chandler. Cincinnati, OH, 1998.

[4]Ocanto, F., R. Alvarez, C. U. d. Navarro, A. Lieb, and C. F. Linares, "Influence of the alkalinity and NO_3^-/Cl^- anionic composition on the synthesis of the cancrinite-sodalite system," *Micropor. Mesopor. Mater.*, **116**(1-3), 318 (2008).

[5]Ocanto, F., E. Figueredo, M. Brikgi, C. U. d. Navarro, and C. F. Linares, "Oxidation-reduction reactions: a novel method in the synthesis of nitrate cancrinite-type zeolites," *Mater. Lett.*, **63**(1) (2009).

[6]Liu, Q., A. Navrotsky, C. F. Jove-Colon, and F. Bonhomme, "Energetics of cancrinite: effect of salt inclusion," *Micropor. Mesopor. Mater.*, **98**(1-3), 227 (2007).

[7]Dumbaugh, W. H., J. C. Lapp, and J. E. Shelby, "Heavy metal oxide glasses," *J. Am. Cer. Soc.*, **75**(9) (1992).

[8]Hruby, A., "Evaluation of glass-forming tendency by means of DTA," *Czech. J. Phys. B (Czechoslovakia)*, **22**(11), 1187 (1972).

[9]Wang, J. S., E. M. Vogel, and E. Snitzer, "Tellurite glass: a new candidate for fiber devices," *Opt. Mater.*, **3**, 187 (1994).

[10]Jantzen, C. M., N. E. Bibler, D. C. Beam, C. L. Crawford, and M. A. Pickett. 1993. *Characterization of the Defense Waste Processing Facility (DWPF) Environmental Assessment (EA) Glass Standard Reference Material (U)*. WSRC-TR-92-346. Savannah River Site, Aiken, SC.

[11]Brady, G. W., "Structure of Tellurium Oxide Glass," *J. Chem. Phys.*, **27**(1) (1957).

[12]Cheremisinov, V. P. and V. P. Zlomanov, "Vibrational spectra and the structure of tellurium dioxide in the crystalline and glass states," *Opt. Spect.*, 110 (1962).

[13]Hocdé, S., S. B. Jiang, X. Peng, N. Peyghambarian, T. Luo, and M. Morrell, "Er^{3+} doped boro-tellurite glasses for 1.5 μm broadband amplification," *Opt. Mater.*, **25**(2) (2004).

[14]Lambson, E. F., G. A. Saunders, B. Bridge, and R. A. Elmallawany, "The Elastic Behavior of TeO$_2$ Glass under Uniaxial and Hydrostatic-Pressure," *J. Non-Cryst. Solids*, **69**(1) (1984).

[15]Stanworth, J. E., "Tellurite Glasses," *J. Soc. Glass. Technol.*, **36**, 217 (1952).

[16]Bürger, H., W. Vogel, and V. Kozhukharov, "IR transmission and properties of glasses in the TeO$_2$−R$_n$O$_m$, R$_n$X$_m$, R$_n$(SO$_4$)$_m$, R$_n$(PO$_3$)$_m$ and B$_2$O$_3$ systems," *Infrared Phys.*, **25**(1-2), 395 (1985).

[17]International, A., "Standard Test Methods for Determining Chemical Durability of Nuclear, Hazardous, and Mixed Waste Glasses and Multiphase Glass Ceramics: The Product Consistency Test (PCT)." In**.** ASTM International, West Conshohocken, PA, 2008.

[18]Ebert, W. L. and S. F. Wolf. 1999. *Round-Robin Testing of a Reference Glass for Low-Activity Waste Forms*. ANL-99/22. Argonne National Laboratory, Argonne, Illinois.

[19]Lindner, G.-G., W. Massa, and D. Reinen, "Structure and properties of hydrothermally synthesized thiosulfate cancrinite," *J. Solid State Chem.*, **117**(2), 386 (1995).

[20]Withers, R. L. and J. G. Thompson, "Modulation wave approach to the structural parameterization and Rietveld refinement of low carnegieite," *Acta Cryst. B*, **49**(4), 614 (1993).

[21]Seemann, H., "Die kristallstruktur des lithiummetasilikates, (Li$_2$SiO$_3$)$_x$," *Acta Cryst.*, **9**(3), 251 (1956).

[22]Hesse, K.-F., "Refinement of the crystal structure of lithium polysilicate," *Acta Cryst. B*, **33**(3), 901 (1977).

[23]Foreman, N. and D. R. Peacor, "Refinement of the nepheline structure at several temperatures," *Z. Kristallogr.*, **132**(1-6), 45 (1970).

[24]Beagley, B., C. M. B. Henderson, and D. Taylor, "The crystal structures of aluminoslicate-sodalites: X-ray diffraction studies and computer modelling," *Mineral. Mag.*, **46**, 459 (1982).

[25]Redman, M. J. and J. H. Chen, "Zinc tellurite glasses," *J. Amer. Ceram. Soc.*, **50**(10), 523 (1967).

[26]Kondratyuk, I. P., L. A. Muradyan, Y. V. Pisarevskii, and V. I. Simonov, "Precision X-ray structure investigation of acoustooptical single crystals of α-TeO$_2$," *Kristallografiya*, **32**(3), 354 (1987).

[27]Beyer, H., "Verfeinerung der kristallstruktur von tellurit, dem rhombischen TeO$_2$," *Zeits. Krist.*, **124**, 228 (1967).

[28]Kulcu, N., *Doga Kim. Ser.*, **11**, 27 (1987).

[29]Knop, O. and G. Demazeau, "The 1-6 weberite Na$_2$Te$_2$O$_7$ and some observations on compounds with the weberite structure," *J. Solid State Chem.*, **39**(1), 94 (1981).

[30]Feger, C. R., G. L. Schimek, and J. W. Kolis, "Hydrothermal synthesis and characterization of M$_2$Te$_3$O$_8$ (M=Mn,Co,Ni,Cu,Zn): a series of compounds with the spiroffite structure," *J. Solid State Chem.*, **143**(2), 246 (1999).

[31] Marinov, M. R., P. G. Sveshtarova, D. A. Stavrakieva, and Y. B. Dimitriev, *Dokl. Bolg. Akad. Nauk.*, **27**(11), 1533 (1974).

[32] Bhat, M. H., M. Kandavel, M. Ganguli, and K. J. Rao, "Li$^+$ ion conductivities in boro-tellurite glasses," *Bull. Mater. Sci.*, **27**(2), 189 (2004).

[33] Rao, K. J. and M. H. Bhat, "Investigation of lithium chloride-lithium borate-tellurium dioxide glasses: an example of complex anionic speciation," *Phys. Chem. Glasses*, **42**(3), 255 (2001).

[34] Dimitriev, Y., E. Kashchieva, I. Ivanova, and D. Khristova, "Liquation in three-component tellurite systems TeO_2-B_2O_3-M_nO_m. M_nO_m=Al_2O_3, Ga_2O_3, Cr_2O_3, CuO, Ag_2O, MoO_3, Sb_2O_3," *Stroit. Mater. Silikat. Prom.*, **24**(9), 24 (1983).

[35] Kashchieva, E. P., "Phase Separation in Tellurite Systems," Thesis**.** Sofia University, Sofia, Bulgaria, 1984.

[36] Kozhukharov, V. S., M. R. Marinov, and J. N. Pavlova, "Phase equilibria and immiscibility in the TeO_2-P_2O_5 system," *J. Mater. Sci.*, **13**, 997 (1978).

[37] Desirena, H., A. Schulzgen, S. Sabet, G. Ramos-Ortiz, E. de la Rosa, and N. Peyghambarian, "Effect of alkali metal oxides R_2O (R = Li, Na, K, Rb and Cs) and network intermediate MO (M = Zn, Mg, Ba and Pb) in tellurite glasses," *Opt. Mater.*, **31**(6), 784 (2009).

[38] Paul, A., "Chemistry of Glasses,*"* 2 ed.: Springer (1989).

[39] Kozhukharov, V., M. Marinov, and G. Grigorova, "Glass-formation ranges in binary tellurite systems containing transition metal oxides," *J. Non-Cryst. Solids*, **28**, 429 (1978).

[40] Fortes, L. M., L. F. Santos, M. C. Goncalves, and R. M. Almeida, "Preparation and characterization of Er^{3+}-doped TeO_2-based oxyhalide glasses," *J. Non-Cryst. Solids*, **324**, 150 (2003).

[41] Bürger, H., K. Kneipp, H. Hobert, W. Vogel, V. Kozhukharov, and S. Neov, "Glass formation, properties and structure in the TeO_2-ZnO system," *J. Non-Cryst. Solids*, **151**, 134 (1992).

[42] Imaoka, M. and T. Yamazaki. 1975. *Glass-Formation Ranges of Ternary Systems. Part 4: Tellurites of a-Group Elements*. Report of the Institution of Industrial Science, Tokyo University, Tokyo, Japan.

[43] Safonov, V. V. and V. N. Tsygankov, "Properties of tellurite/halide glasses of the $NdCl_3$-TeO_2-WO_3 system," *Russ. J. Inorg. Chem.*, **50**(11), 1740 (2005).

[44] Safonov, V. V., "The $NdCl_3$-TeO_2-WO_3 system," *Russ. J. Inorg. Chem.*, **50**(11), 1737 (2005).

[45] Champarnaud-Mesjard, J.-C., P. Thomas, P. Marchet, B. Frit, A. Chagraoui, and A. Tairi, "Glass formation study in the Bi_2O_3-TeO_2-WO_3 system,*"* pp. 289-292, *Proc. of the 7th Moroccan Meeting on Solid State Chemistry*, **(23)1-2**. Marrakesh, Morocco, 1996.

[46] Yakhkind, A. K. and S. A. Chebotarev, "Density and thermal expansion of ternary tellurite glasses with barium- and cadmium halides," *Fiz. Khim. Stekla (USSR)*, **9**(3), 301 (1983).

[47] Blanchandin, S., P. Marchet, P. Thomas, J. C. Champarnaud-Mesjard, B. Frit, and A. Chagraoui, "New investigations within the TeO2-WO3 system: phase equilibrium diagram and glass crystallization," *J Mater Sci*, **34**(17) (1999).

[48] Kozhukharov, V., M. Marinov, I. Gugov, H. Burger, and W. Vogel, "A new family of tellurite glasses, Part 1 Glass formation," *J. Mater. Sci.*, **18**(5), 1557 (1983).

[49] Sekiya, T., N. Mochida, and S. Ogawa, "Structural Study of WO_3-TeO_2 glasses," *J. Non-Cryst. Solids*, **176**, 105 (1994).

[50] Sekiya, T., N. Mochida, and S. Ogawa, "Structural Study of MoO_3-TeO_2 glasses," *J. Non-Cryst. Solids*, **185**, 135 (1995).

[51] Durga, D. K. and N. Veeraiah, "Physical properties of ZnF_2-As_2O_3-TeO_2 glasses doped with Cr^{3+} ions," *Phys. B-Cond. Mat.*, **324**(1-4) (2002).

Appendix A: Tellurite Glass Literature Review

A-1. Borotellurite and/or Boroaluminotellurite Glasses

Hocdé et al.[13] proposed the use of borotellurite glass doped with Er^{3+} in 1.5 µm broadband amplification. Glasses consisted of TeO_2 (60–65 mol%), B_2O_3 (15 mol%), and Na_2O (10–25 mol%), and replacements of Na_2O and TeO_2 were made with GeO_2 (5–7 mol%) and/or Al_2O_3 (5–10 mol%) to change the refractive index, thermal stability and chemical durability of the glass. One glass was made consisting of TeO_2, WO_3 and K_2O, which will be discussed in Section A-4. Mixtures were heated in a furnace at 700–800°C. The crucible material is not specified. The melt was kept under nitrogen gas flowing at a rate of 10 liters per minute to create a difference of water pressure and drive water out of the glass, helping to reduce the hydroxyl impurities inherent in the source chemicals, which reduce the light-emitting properties of Er^{3+} ions. There is no mention of the duration of this treatment. Melts were then cast in preheated molds (the mold material is not specified) and annealed for 2 hours at the T_g of each composition, and then cooled slowly to room temperature for 15 hours. Chemical durability was tested for each glass. Samples were cut and polished to dimensions of approximately $4 \times 16 \times 24$ mm, weighed carefully, immersed in boiling water for 15 min intervals and reweighed after each immersion to determine weight loss. Observations about glass formulation were reported:

- Glasses with > 70 mol% TeO_2 had a strong tendency to crystallize upon cooling.

- Compositions with > 20 mol% B_2O_3 caused phase separation in the glass.

- Network modifiers (e.g., Na_2O) led to a stable tellurite glass but tend to deteriorate chemical durability and led to crystallization at elevated concentrations.

- The replacement of Na_2O with GeO_2 increased T_g, refractive index and thermal stability of the glass.

- Na_2O replacement with Al_2O_3 also increased the T_g and the refractive index, improved thermal stability, and significantly improved chemical durability. For example, with TeO_2, GeO_2 and B_2O_3 compositions remaining constant (60, 5 and 15 mol%, respectively), exchanging 5 and 10 mol% Na_2O with Al_2O_3 decreased the weight loss after 30 min from 0.6 mg/mm^2 to 0.19 and < 0.01 mg/mm^2, respectively.

- For Al_2O_3 content exceeding 15 mol%, the melting temperature of 700–800°C is too high and decomposition and crystallization occur, therefore addition of Al_2O_3 to this system should be limited to < 15 mol%. Among chemically durable tellurite glasses, Al_2O_3 appears to be a promising additive for borotellurite glasses.

- The glass composition of 75 mass% TeO_2, 8 mass% B_2O_3, 8 mass% Al_2O_3, 5 mass% Na_2O, and 4 mass% GeO_2, showed the best durability, with a mass loss of 4.85 g/m^2 in 1 hr (116 g/m^2/day) upon immersion in boiling water.

Rao and Bhat[32] and Bhat et al.[33] looked at alkali borotellurite glasses with the addition of up to 10 mol% of LiCl with $T_g = 366°C$. Rao and Bhat focused their efforts on understanding the structure of borotellurite glasses. They observed that the LiCl itself acted as a plasticizer, opening up the network, and was determined to be in clusters throughout the glass. These studies did not report glass durability.

Dimitriev et al.[34] and Kashchieva[35] researched the glass formation region of the TeO_2-B_2O_3-Al_2O_3 ternary system. These ternary diagrams agree very well with one another (see Figure A.1) and demonstrate a glass formation region limited by Al_2O_3 loading at ~ 5–20 mass% with B_2O_3 as high as ~ 65 mass%. Dimitriev et al.[34] melted 5 g batches in porcelain and alumina crucibles at 1100°C and cooled at a rate of ~ 100°C/min.
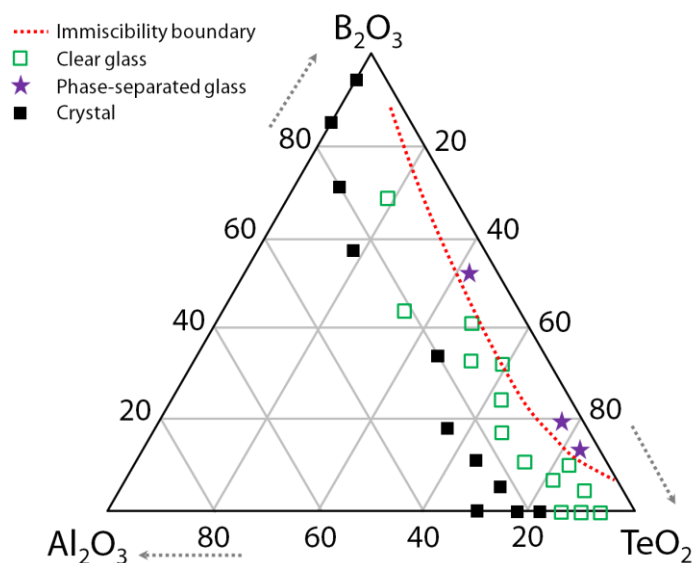
Figure A.1. Glass formation region of TeO_2-Al_2O_3-B_2O_3 glasses according to Kashchieva.[35]

A-2. Phosphotellurite Glasses

Kozhukharov *et al*.[36] investigated the TeO_2-P_2O_5 binary system for regions of miscibility and immiscibility. From this study, it was determined that the immiscibility confines the glass formation region boundary at ≤ 25.8 mol% P_2O_5. Glasses, in 10 g quantities, were prepared by pre-calcination at 450°C in air in porcelain crucibles and then melted in dry air for 15–20 min at 800–950°C, depending on composition. They report that a liquid-liquid phase separation was observed visually with the increase in P_2O_5 to > 30 mol%. In Figure A.2, "a" denotes a homogeneous liquid producing clear glass, "b" denotes a liquid with "special" structure (i.e., with an extremely high dispersion of the existing liquid phases), and "c" denotes a liquid with micro-heterogeneous structure (i.e., non-homogeneous glass). According to Kozhukharov *et al*., the solubility limit of P_2O_5 in this binary for producing a clear, homogeneous glass is ~3–15 mol% (2.7–13.6 mass%) (Figure A.2, Region "a"). The ten different phases (including crystalline forms) observed by Kozhukharov *et al*. are also presented to the right of the diagram.
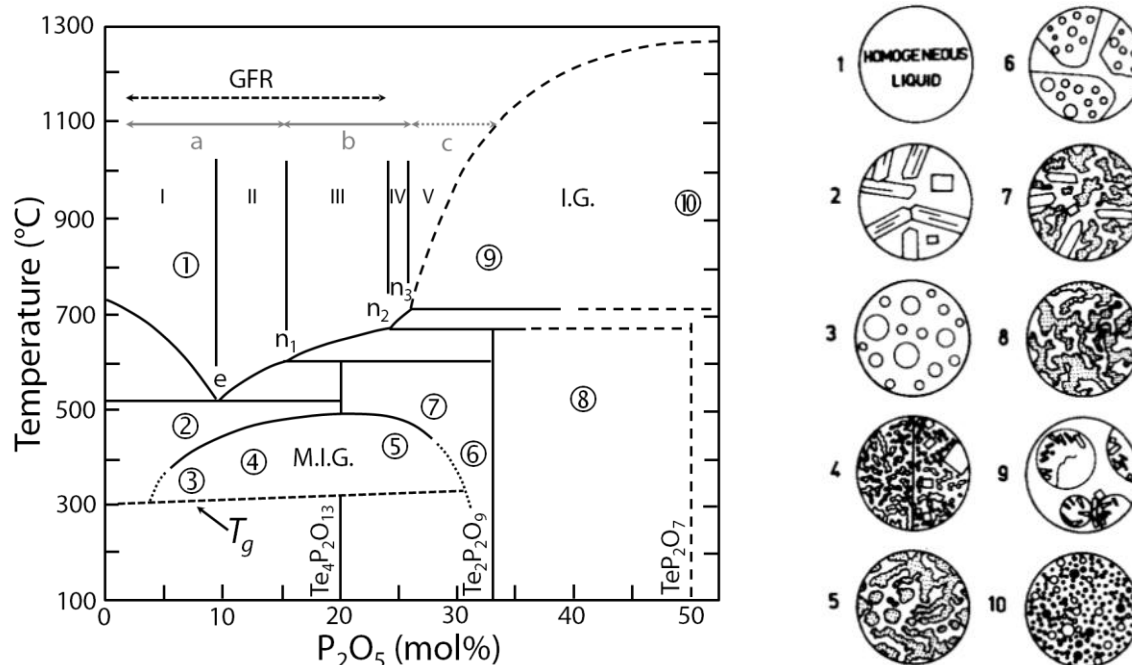
Figure A.2. Glass formation region of TeO_2-P_2O_5 binary system as taken from Kozhukharov et al.[36]

Stanworth[15] made several glasses with TeO_2, PbO, and P_2O_5 with increasing percentages of phosphate introduced as lead phosphate. The glasses were melted in zirconia crucibles. The physical properties of the glass with the highest percentage of P_2O_5 (44.1 mass% TeO_2, 42.5 mass% PbO, and 13.4 mass% P_2O_5,) were recorded: T_g = 335°C; the release rate of this glass was 0.02 g/m²/day in the moist environment, and in the tests for resistance to acid and alkali, slight and heavy attack were observed, respectively.

Bürger et al.[16] investigated the infrared (IR) transmission and other properties of a variety of tellurite glasses. Batches (50–200 g) of reagent-grade TeO_2 and pre-dried oxides, sulfates, metaphosphates and halides were melted directly in Au and Pt crucibles (Al_2O_3 crucibles were also used in a few cases). Melting was carried out in a dry air atmosphere in a SiC furnace at 800–1050°C for 1–2 h. *Oxygen gas (O_2) was bubbled through the melt for phosphotellurite glasses to prevent reduction of TeO_2 to Te*. The melts were quenched from ~ 600°C at rates varying between 8°C/s and 2°C/min. Two glasses were made with metaphosphates: 69.5 mass% $Pb(PO_3)_2$ and 65 mass% $Ba(PO_3)_2$ with the balance TeO_2, that had deformation temperatures of 355°C and 410°C, respectively.

A-3. Non-Transition Metal Oxide Tellurite Glasses

Stanworth[15] performed an expansive study on the TeO_2-PbO and TeO_2-BaO binary systems and TeO_2-PbO-X ternary systems where X was either a glass former (i.e., B_2O_3) or modifier (e.g., MoO_3, P_2O_5, Nb_2O_3, WO_3, Na_2O, Li_2O, and BaO). Glasses were melted in batches of various sizes in ceramic crucibles (alumina, fused-silica and zirconia) at 950–1000°C. The quenching method is not mentioned; it is assumed that the glasses were poured on a steel or other metal plate as is the common quench method with such glasses.

The glasses were placed in a sealed chamber at 50–55°C under saturated water vapor; after three weeks, the glasses were dried and the weight loss determined. The most efficient binary PbO-TeO_2 glass (i.e., high chemical durability, glass processability) was a binary glass with 83.2 mol% (78 mass%) TeO_2 and 16.8 mol% (22 mass%) PbO, respectively with a release rate of 0.005 g/m²/day. The glass performances were consistently worse with the addition of modifiers to the TeO_2-PbO binary system in the order listed above (i.e., $MoO_3 \rightarrow P_2O_5 \rightarrow Nb_2O_5 \rightarrow La_2O_3 \rightarrow WO_3$) though release rates were still very low at ≤ 0.04 g/m²/day for the modifier with the highest release rate in this series, WO_3.

Another binary glass with 86.4 mol% (82 mass%) TeO_2 and 13.6 mol% (18 mass%) PbO exhibited a release rate of 0.02 $g/m^2/day$, four times the release rate of the other TeO_2-PbO glass mentioned above. One binary barium tellurite glass (83.5 mol% of TeO_2 and 16.5 mol% BaO) was subjected to the water durability test, and the release rate was 4.4 $g/m^2/day$, which indicates it is significantly less durable the binary TeO_2-PbO glass mentioned above. $T_g \geq 280°C$ for most glasses in this study except for two glasses:

- TeO_2-PbO-V_2O_5 glass (29.4, 20.5 and 50.1 mass%, respectively)

- TeO_2-PbO glasses with 2–4 mass% Li_2O or Na_2O.

Stanworth[15] also looked at TeO_2-PbO-P_2O_5 ternary glasses and found that the addition of P_2O_5 to the TeO_2-PbO binary produced glass with a lower thermal expansion coefficient and a higher deformation temperature (335°C). The composition of this glass was 44.1 mass% TeO_2, 42.5 mass% PbO, and 13.4 mass% P_2O_5.

Desirena et al.[37] studied TeO_2 glasses with alkali and alkaline earth oxides. The physical and chemical properties of TeO_2-MO-R_2O glasses (M = Zn, Mg, Ba, Pb; R = Li, Na, K, Rb, Cs) were systematically characterized. Glass compositions were 70 mol% TeO_2, 20 mol% MO, and 10 mol% R_2O. Chemical constituents were mixed together in calculated quantities in a glass dish and melted at 900°C for 1 hour in Al_2O_3 crucibles. Glass samples were cut and polished into 125 mm^3 cubes, carefully weighed and placed in a 200 mL beaker of boiling deionized water for 1 hour. Samples were removed, washed with acetone and dried at 80°C for 1 hour in a furnace and the weight loss was determined. The four glasses that exhibited the lowest release rates (< 3 $g/m^2/day$) out of all glasses tested in this study had compositions (mass%) of [68.7 % TeO_2, 27.5 % PbO, 3.8 % Na_2O]; [70.1 % TeO_2, 28.0 % PbO, 1.9 % Li_2O]; [83.3 % TeO_2, 12.1 % ZnO, 4.6 % Na_2O]; and [85.3 % TeO_2, 12.4 % ZnO, 2.3 % Li_2O]. T_g was 275–310°C for the listed glass compositions in this study.

One caveat with this study: since these glasses were melted in Al_2O_3 crucibles, and the glasses were not chemically analyzed following melting, there is a chance that some of the Al_2O_3 from the crucible wall could have dissolved into the melt as with Stanworth's glasses and aided in glass formation.[15]

Paul[38] presented a TeO_2-PbO binary phase diagram suggesting that the glass formation region is at PbO concentrations of ~ 4–18.5 mol% (5–24 mass%). A similar diagram was presented by Marinov et al.[31] (see Figure A.3).

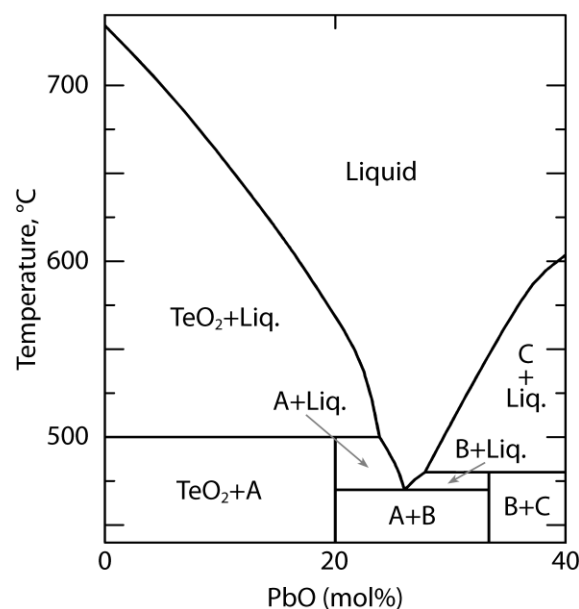Figure A.3. Glass formation region of TeO_2-PbO for compositions of $4TeO_2$:PbO (A), $2TeO_2$:PbO (B), and $3TeO_2$:2PbO (C) as presented by Marinov et al.[31]

A-4. Transition Metal Oxide Tellurite Glasses

Redman and Chen[25] investigated optical properties of zinc tellurite glasses. They demonstrated optical transmission in the range of 0.38–6.6 μm with two absorption bands in the IR. They reported that the optical surfaces of the glasses were not affected by cold water, were slowly attacked by boiling water and by dilute acids, and rapidly attacked by strong acids and dilute alkali.

Kozhukarov et al.[39] investigated the glass-forming ability of binary tellurite glasses containing transition metal oxides. Batches were accurately weighed at 2 g, homogenized, melted at 800–1000°C in quartz crucibles and cooled on a copper plate at room temperature. Melts of TeO_2 with V_2O_5, MoO_3, WO_3, and ZnO exhibited glass-forming ability over wide composition ranges (8.5–61.2 mass%, 12.8–56 mass%, 15.2–42 mass%, and 4.9–25.4 mass%, respectively, on an oxide basis). No additional data were reported for these glasses. This demonstrates excellent glass formability of these particular additives in a binary system with tellurite. However, analysis of the glass composition after melting was not performed, and it is uncertain what fraction of SiO_2 from the glass crucibles dissolved into the melts.

Fortes et al.[40] prepared bulk oxyhalide glasses in the TeO_2-ZnO-ZnX_2 and TeO_2-PbO-PbX_2 systems (X = Cl, Br, I) and investigated glass formability ranges, as well as density for each glass. Batches of ~ 5 g (99.99% purity TeO_2, $ZnCl_2$ and $ZnBr_2$; > 98% purity for other compounds) were weighed and stored in a vacuum furnace at ~ 100°C to minimize adsorbed water content due to the hygroscopicity of the halide compounds. In a N_2 glove box, mixtures were heated at ~ 200 for 2 hours for further dehydration. Subsequent melting was carried out at ~ 800°C for about one hour. The melts were poured into stainless steel molds preheated to 240°C and annealed at this temperature for about 12 hours. Some noted experimental difficulties included the preferential volatilization of certain species during the melting process, which affected the final composition of the glass and the chemical reactivity of the melts with the crucible materials. Traces of Al were found in the preliminary 5 g batches melted in alumina crucibles. The TeO_2–ZnO–$ZnCl_2$ system exhibited the highest glass-forming ability. The glass forming ability of the systems with Pb compounds was limited. Chemical durability was not assessed in this study.

Bürger et al.[41] investigated the glass formation ability and structure of the TeO_2-ZnO binary glass system. Glasses with 17.4–37.2 mol% ZnO were melted in gold crucibles at 860–950°C for 45 minutes and cooled at rates of ~1°C/min and ~10°C/s by pouring into graphite and copper molds, respectively. The glass formation ranges at these cooling rates were 20–30 mol% (11.3–17.9 mass%) ZnO for 1°C/min cooling and 17.1–37.3 mol% (9.5–23.3 mass%) ZnO for 10°C/s cooling. Bürger et al. demonstrated greater glass stability against devitrification for glass compositions around the eutectic and above the liquidus line for primary crystallization of $Zn_2Te_3O_8$. The upper limit of the glass-formation region (GFR) at a cooling rate 10°C/s correlates with a peritectic point of $ZnTeO_3$ and with the isopleths of the $Zn_2Te_3O_8$ compound as well. Chemical durability for these glasses was not reported.
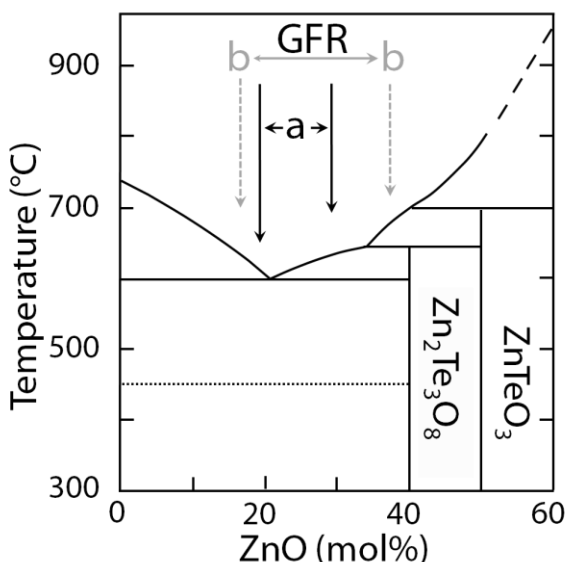
Figure A.4. Glass formation region (GFR) of TeO_2-ZnO binary glasses from Bürger *et al*.[41] The data presented for the binary system includes data for different quench rates (a = ~1°C/min, b = ~10°C/s).

Tungstenate (WO_3) has often been used as a transition-metal network intermediate in tellurite glasses. Four separate studies[42–46] show that the GFR can be conservatively estimated at 15–28 mass% of WO_3 in the TeO_2-WO_3 binary. A liberal range according to these four studies is 5–45 mass% WO_3, suggesting that the methods of preparation and quenching of these glasses led to different crystallization phenomena, though Imaoka[42] demonstrated a GFR of 5–45 mass% WO_3 when quenching in air. A phase diagram with the different GFRs is presented in Figure A.5.

Hocdé *et al*.[13] manufactured a glass consisting of 57.1 mass% TeO_2, 34.5 mass% WO_3, and 8.4 mass% K_2O, in addition to several borotellurite glasses. The T_g and T_c of this glass were 352°C and 432°C, respectively. After 30 minutes in boiling water, the reported weight loss for this glass was 30 g/m^2, which was significantly lower than most of the borotellurite glasses analyzed. This result suggests the viability of WO_3 as an additive in the synthesis of chemically durable glass products for the current application with decent alkali loading.

Blanchandin *et al*.[47] constructed a TeO_2-WO_3 phase diagram by heating the mixtures in gold crucibles at 750°C for 12 hours and then holding at 480°C for 24 hours. They found the eutectic composition to be 22 ± 1 mol% (or 29 ± 1.2 mass%) WO_3 at 622°C with a very steep slope at compositions with WO_3 > 22 ±1 mol%. This suggests that the lowest processing temperature could be achieved at ~ 29 mass% WO_3 and that compositions with lower WO_3 content could still be melted at reasonable temperatures.
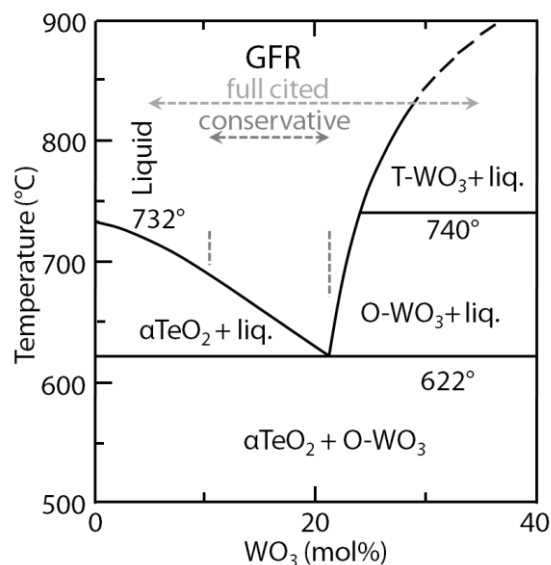
Figure A.5. TeO$_2$-WO$_3$ Phase diagram as taken from Blanchandin *et al*.[47]

A-5. Overview and Simple Candidate Selection

It is apparent from this literature review that tellurite glass has been used extensively as a host for halides and has a large processing window with the ability to accommodate a long list of glass formers, modifiers, and intermediates. Following the expanded literature review, five primary systems were chosen for further exploration as hosts for the XCl_{20} Echem salts; selection was based on attractive chemical and physical properties as described below. These systems include TeO$_2$ + X where X = PbO, Al$_2$O$_3$ + B$_2$O$_3$, WO$_3$, P$_2$O$_5$, and ZnO.

A-5.1 TeO$_2$-PbO system

The results reported by Stanworth[15] and Desirena *et al*.[37] suggested that PbO is a promising additive in TeO$_2$ glasses to improve chemical durability. Reported glasses exhibited relatively low total release rates (i.e., < 8 g/m^2/day) and reasonably high T_g (i.e., $\geq$ 280°C). Though chloride solubility was not investigated in these studies, PbO seemed to be promising for formulating a chemically durable tellurite glass to immobilize the Echem spent salt. As per Stanworth's data described previously in Section A-3, the TeO$_2$/PbO glass selected for further study was 78 mass% TeO$_2$ and 22 mass% PbO due to low reported chemical release rates. The initial temperature used for melting glasses of this system was 950°C, as documented by Stanworth.[15] This proved too hot on account of PbO volatility. A lower melting temperature of 705°C was selected based on the findings of Marinov *et al*.[31]

A-5.2   TeO$_2$-Al$_2$O$_3$-B$_2$O$_3$ System

Alumina and boria are often used as additives to silicate glasses in order to improve processability and glass properties. Boria acts as a flux and is added to silicate glasses to reduce the melting temperature and lower the viscosity of the melt. As discussed in section A-1, Hocdé *et al*.[13] observed that the addition of alumina to tellurite glasses was "…found to be particularly effective at improving chemical durability…however when the content of Al$_2$O$_3$ [exceeded] 15 mol%, the melting temperature of the glass [became] too high and decomposition and crystallization [occurred]." According to Hocdé *et al*.,[13] the addition of alumina also had the tendency to increase T_g and improve thermal stability, both important attributes for a waste form. According to the ternary diagram in Figure A.1, the starting point in this system was 82.2 mass% TeO$_2$, 8.8 mass% Al$_2$O$_3$ and 9.0 mass% B$_2$O$_3$. As discussed in Section A-1, the addition of GeO$_2$ and Na$_2$O will be considered if problems arise (such as poor glass formability or durability) from the basic ternary system or to improve the glass properties following an initial PCT test. Like alumina, the addition of GeO$_2$ could be used to increase the T_g and increase thermal stability. The

initial melting temperature used for making TeO_2-Al_2O_3-B_2O_3 scoping test glasses was 800°C, the maximum temperature used by Hocdé et al.[13]

A-5.3   TeO₂-WO₃ System

Several glass formation studies[42-46] have been done in TeO_2-WO_3 ternary systems which overlap with the TeO_2-WO_3 binary, suggesting that a conservative estimate of the GFR in the TeO_2-WO_3 binary system would be 15–28 mass% of WO_3. These studies revealed good solubility of rare-earth chlorides[43-44] and alkaline earth chlorides.[46] Hocdé et al.[13] presented durability data on a TeO_2-WO_3-K_2O glass that showed significant durability improvement over the borotellurite glasses that they tested, suggesting that WO_3 could improve glass durability. After reviewing the methods used for the other studies and the phase diagram by Blanchandin et al.,[47] the first composition chosen for a TeO_2-WO_3 glass was 25 mass% WO_3, melted at 700°C.

A-5.4   TeO₂-P₂O₅ System

Kozhukharov et al.,[48] demonstrated the use of P_2O_5 as an additive to TeO_2, which resulted in better glass formation than the borotellurite system. Also, Stanworth[15] demonstrated that P_2O_5 can have good chemical durability when incorporated into a lead tellurite glass. Bürger et al.[16] demonstrated the need to bubble oxygen through the melt when melting phosphotellurite glasses in order to prevent the reduction $Te^{+4} \rightarrow Te^0$, which will be considered if such reduction is observed during experimental processing. After consideration of the TeO_2-P_2O_5 binary phase diagram (see Figure A.2), the glass formation region is 0–15 mol% (13.5 mass%) P_2O_5 and thus the starting point chosen for this work was 10 mass% P_2O_5, processed at 630°C.

A-5.5   TeO₂-ZnO System

Several researchers studied glass formation in TeO_2-ZnO binary and ternary systems, a few of which were included in this current study;[39-41] review of the data, on the glass formation region of the TeO_2-ZnO binary was inconclusive. Kozhukharov et al.[39] presented the region as 4.9–25.4 mass% ZnO, Fortes et al.[40] presented the region as 0–43.34 mass% ZnO, and Burger et al.[41] presented the region as 9.5–23.3 mass%. For the current study, the most conservative values (Burger et al.[41]) were implemented in experimental design. The glasses presented in this study show good glass formation when low quenching rates were implemented, i.e., as low as 1°C/min for glasses in the range of 9.5–23.3 mass% ZnO.[41] After consideration of the phase diagram (see Figure A.4) and the literature data, the initial composition selected for this system was 18 mass% ZnO (balance TeO_2) melted at 725°C.

A-5.6   Other Simple Candidate Systems

A-5.6.1   TeO₂-MO$_x$ (M = Transition or Non-Transition Metal)

A few different studies reviewed included glasses made with other transition metal oxides (i.e., MoO_3, WO_3, V_2O_5, Nb_2O_5)[9,13,15,37,45,49-50] and/or non-transition metal oxides (i.e., Bi_2O_3, As_2O_5, GeO_2)[13,45,51] that showed promise for improving glass performance and other properties. Stanworth[15] concluded from his study that the glass performance of MoO_3-containing TeO_2 glasses was higher than the phosphotellurite glasses. Durga and Veeraiah[51] showed glasses composed of 50 TeO_2 + 40 ZnF_2 + (10-x)*As_2O_3 + x*Cr_2O_3 (values in mass%) had moderate performance. In this study, glasses where $x = 0.3$ and 0.6 mass% had the maximum and minimum dissociation rates of 43.2 and 2.4 g/m^2/day, respectively. The best composition for the current application in this quaternary system is $x = 0.6$ mass% or 50 mass% TeO_2, 40 mass% ZnF_2, 9.4 mass% As_2O_5, and 0.06 mass% Cr_2O_3, with maximum T_g and minimum release rate.

A-5.7   TeO₂-MCl$_x$ (M = Transition or Non-Transition Metal)

A few other studies[40,48] discussed glasses made with metal chlorides (i.e., $ZnCl_2$, $PbCl_2$, etc.) as an additive, which seemed to improve glass formation and/or durability. Fortes et al.[40] discussed the addition of $ZnCl_2$ to the TeO_2-ZnO binary system at very high fractions (up to 80 mol%). The glass with

the largest $T_x - T_g$ (without crystallinity) had a composition of 30-20-50 mol% TeO_2-ZnO-$ZnCl_2$, respectively, with a value of 293°C suggesting glass formation without requiring a fast quench, although the exact melting temperature was unknown. Kozhukharov *et al.*,[48] demonstrated $BaCl_2$ and $PbCl_2$ solubility in TeO_2-P_2O_5 glasses.

Appendix B: Source Chemicals for Tellurite Glass Batching

B-1. Loss on Drying & Moisture Analysis Methods

The source chemical stocks for the Echem salts (see Table B 1) were subjected to a loss on drying (LOD) test to account for hydration in batching waste-loaded glasses. Samples of $\geq$ 1 g in uncovered porcelain crucibles were heat treated at 105°C in a ventilated oven for 24-hour periods. Samples were considered dry when the mass did not change significantly between two 24-hour heat treatments. A hydration correction factor, F_{loss}, was calculated according to the expression: $F_{loss} = 1 / m_{dry}$, where m_{dry} is the dry weight of the salt. The desired mass of salt was multiplied by this factor to determine the amount of hydrated salt to add to the batch to achieve the desired mass of salt in the glass.

A Mettler-Toledo HR83 moisture analyzer was also used to measure the moisture content of the salts used to batch waste-loaded glasses. A standard drying program was used with a drying temperature of 140°C and the switch-off mode 5, to allow for samples that dried slowly; in switch-off mode 5, samples were held at this temperature until the $\Delta m / \Delta t$ was negligible.

Table B 1. Source chemicals used in batching tellurite glasses. ACS denotes that the chemical meets the specifications of the American Chemical Society. REO denotes the content of rare earth oxide.

Chemical Name	Formula	PNL Barcode	Manufacturer	Purity	Lot No.	Stock #	Mesh size
barium chloride dihydrate	$BaCl_2 \cdot 2H_2O$	129042	Sigma	ACS Reagent	25H0268	n/a	
cerium (III) chloride hydrate	$CeCl_3 \cdot xH_2O$	256536	REacton (Alfa Aesar)	99.9% (REO)	L17P33	11325	
cesium chloride	CsCl	34287	Argent Chemical Laboratories, Inc.	ACS Reagent	810120	n/a	
lanthanum chloride 7-hydrate	$LaCl_3 \cdot 7H_2O$	5238	JT Baker Chemical Co.	'Baker Analyzed' Reagent	322338	n/a	
lithium chloride	LiCl	5984	Mallinckrodt	Analytical Reagent	Lot anal. on bottle	n/a	
neodymium chloride hydrate	$NdCl_3 \cdot xH_2O$	307830	REacton (Alfa Aesar)	99.9% (REO)	H21T060	11251	
potassium chloride	KCl	45370	Chem West	ACS Reagent	Lot anal. on bottle	n/a	
praseodymium chloride hydrate	$PrCl_3 \cdot xH_2O$	307828	REacton (Alfa Aesar)	99.9% (REO)	C31U003	11237	
samarium chloride hydrate	$SmCl_3 \cdot xH_2O$	307829	REacton (Alfa Aesar)	99.9% (REO)	C06U028	11231	
sodium chloride	NaCl	111184	Aldrich	99+% ACS Reagent	12926EN	n/a	
tellurium (IV) oxide	TeO_2	191527	Puratronic (Alfa Aesar)	99.9995%	22389	10882	
tellurium (IV) oxide	TeO_2	307851	Puratronic (Alfa Aesar)	99.9995%	23424	10882	
aluminum oxide	Al_2O_3	118316	CERAC Inc.	typically 99.999%	16067-A-3	A-1188	-40
aluminum oxide	Al_2O_3	67135	CERAC Inc.	typically 99.5%	7087	A-1215	-325
boric oxide	B_2O_3	None	20Mule Team US Borax Inc.	technical grade	not listed	n/a	60
lead oxide, mono	PbO	67607	Fischer		7087	n/a	
phosphorus (V) oxide	P_2O_5	308014	Alfa Aesar	99.99%	L11T031	89966	
silicon dioxide	SiO_2	116851	Atomergic Chemetals Corp.	99.999%	J1495	n/a	
tungsten (VI) oxide	WO_3	196880	Alfa Aesar	99.8% metals basis	L13K02	11828	
zinc oxide	ZnO	88741	ESPI Metals	99.999%	Q1140	n/a	-325

B-2. Loss on Drying (LOD) & Moisture Analysis Results

Moisture analysis results showed that the LOD values measured using the porcelain crucibles were found to be within 2% of the total mass of the added chlorides. The LOD values differed for the two methods; thus in FY2011, careful consideration will be taken to make sure that the most accurate LOD values for the chlorides will be used for batch sheet calculations. As seen in Figure B 1, the mass% of dry content in the additives differed depending on the method used to determine the value. It is probably most prudent to use the values obtained by the LOD though a loss on ignition (heating additives to 500°C for an extended time) will be performed on these additives in FY2011 to see where that data will fit on this chart.
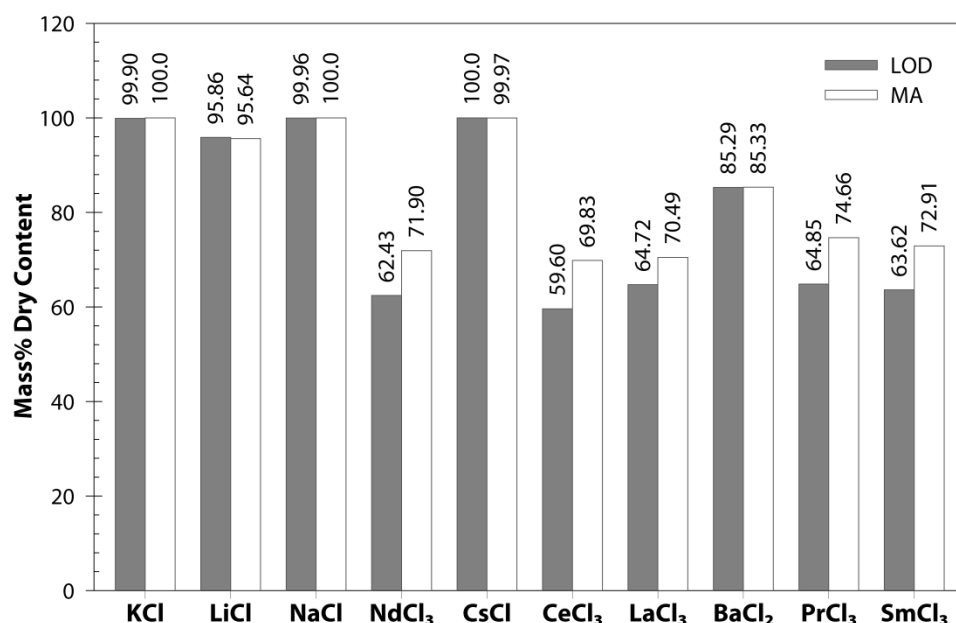

Figure B 1. Comparative plot of dry content values found by the LOD test and the Moisture Analysis results.

Appendix C: PCT Normalized Release Values for Tellurite Glasses

Table C 1. Summary of PCT normalized release of FY2010 tellurite glasses for species detected by IC and ICP-OES. Averages are listed along with standard deviations in parenthesis directly below.

Glass	Composition, mass%	Average Normalized Release, NL_i, g/m^2									
		Cl g/m²	Al g/m²	B g/m²	P g/m²	Pb g/m²	Zn g/m²	Ba g/m²	K g/m²	Li g/m²	Na g/m²
LRM		–	0.123	0.498	0.146	0.102	–	–	0.130	–	0.504
		(–)	(0.001)	(0.007)	(0.003)	(0.015)	(–)	(–)	(0.007)	(–)	(0.014)
P-8	78TeO$_2$–22PbO	–	–	–	–	–	–	–	–	–	–
		(–)	(–)	(–)	(–)	(–)	(–)	(–)	(–)	(–)	(–)
P-11	70.2TeO$_2$–19.8PbO–10XCl$_{20}$	0.528	–	–	–	–	–	0.099	0.298	1.002	0.478
		(0.009)	(–)	(–)	(–)	(–)	(–)	(0.004)	(0.013)	(0.006)	(0.006)
P-7	82.2TeO$_2$–8.8Al$_2$O$_3$–9B$_2$O$_3$	–	–	3.980	–	–	–	–	–	–	–
		(–)	(–)	(0.038)	(–)	(–)	(–)	(–)	(–)	(–)	(–)
P-2	74TeO$_2$–7.9Al$_2$O$_3$–8.1B$_2$O$_3$–10XCl$_{20}$	3.845	0.007	2.145	–	–	–	2.104	3.449	5.498	6.715
		(0.103)	(0.001)	(0.083)	(–)	(–)	(–)	(0.106)	(0.132)	(0.237)	(0.26)
P-9	75TeO$_2$–25WO$_3$	–	–	–	–	–	–	–	–	–	–
		(–)	(–)	(–)	(–)	(–)	(–)	(–)	(–)	(–)	(–)
P-12	67.5TeO$_2$–22.5WO$_3$–10XCl$_{20}$	4.617	–	–	–	–	–	–	2.852	7.246	10.256
		(0.016)	(–)	(–)	(–)	(–)	(–)	(–)	(0.039)	(0.202)	(0.148)
P-5	91TeO$_2$–9P$_2$O$_5$	–	–	–	80.778	–	–	–	–	–	–
		(–)	(–)	(–)	(2.688)	(–)	(–)	(–)	(–)	(–)	(–)
P-14	81.9TeO$_2$–8.1P$_2$O$_5$–10XCl$_{20}$	30.296	–	–	76.472	–	–	72.557	88.361	82.652	85.993
		(2.914)	(–)	(–)	(4.267)	(–)	(–)	(2.056)	(7.097)	(7.301)	(5.918)
P-4	82TeO$_2$–18ZnO	–	–	–	–	–	0.166	–	–	–	–
		(–)	(–)	(–)	(–)	(–)	(0.005)	(–)	(–)	(–)	(–)
P-13	73.8TeO$_2$–16.2ZnO–10XCl$_{20}$	84.747	–	–	–	–	3.100	76.561	89.092	85.278	88.913
		(0.518)	(–)	(–)	(–)	(–)	(0.015)	(2.434)	(1.045)	(4.817)	(0.859)

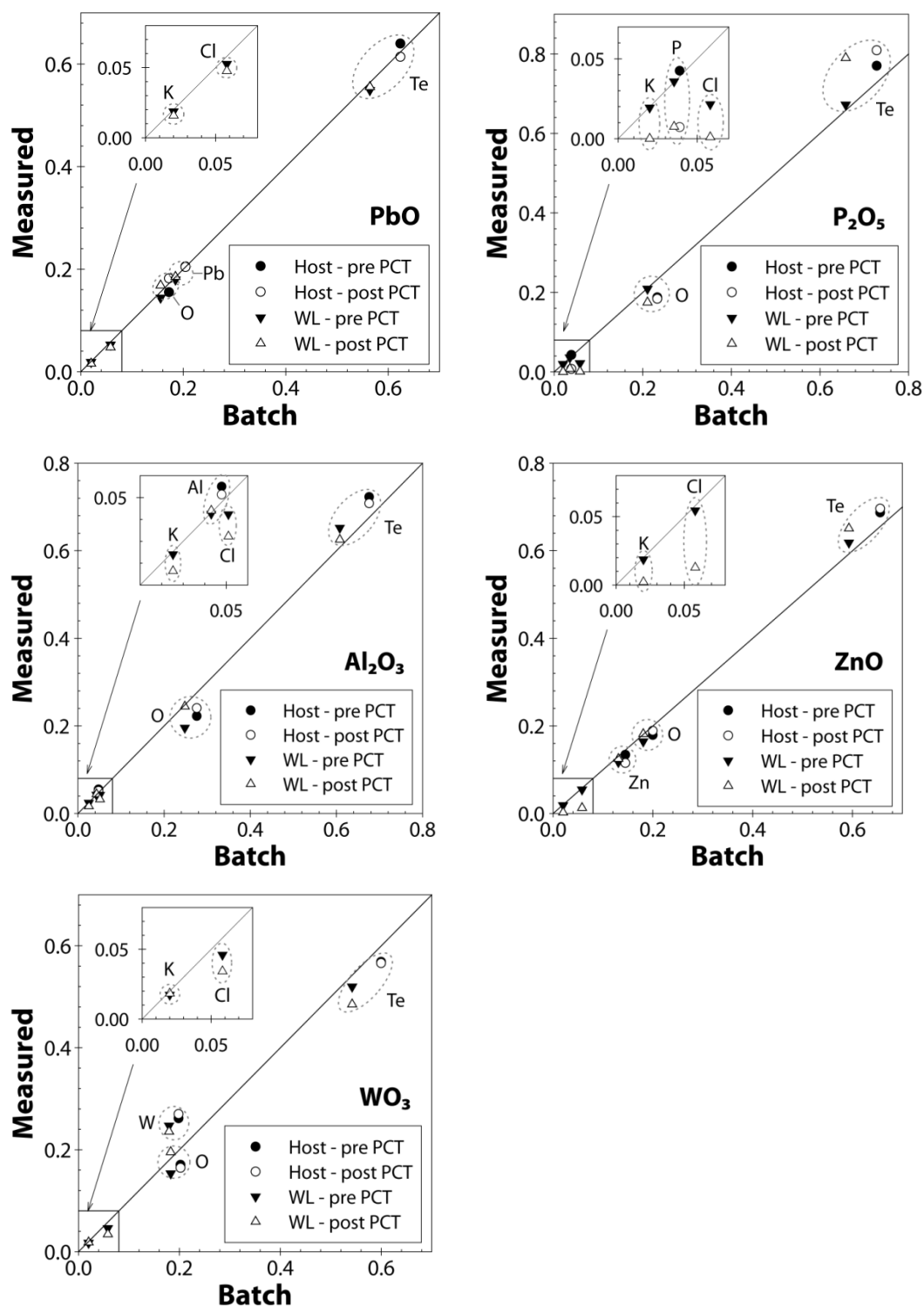# Appendix D: EDS Comparison Plots for Tellurite Glasses

Figure D 1. EDS plots comparing targeted compositions ("Batch") with measured ("Measured") compositions for measureable species.

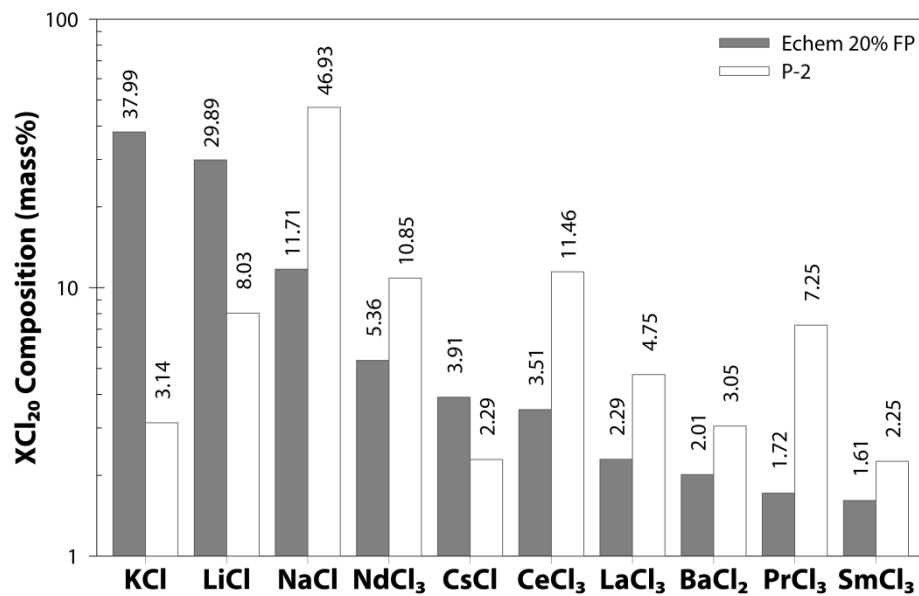# Appendix E: Comparison of XCl$_y$ used for Tellurite Glass P-2

Figure E 1. Comparative plot showing the difference between the correct ("Echem 20% FP" or XCl_{20}) and incorrect ("P-2") waste stream used for batching Glass P-2, the Al_2O_3-B_2O_3 glass with 10% mixed chlorides (XCl_y).